



HAL
open science

River network routing on the NHDPlus dataset

Cédric H. David, David R. Maidment, Guo-Yue Niu, Zong-Liang Yang,
Florence Habets, Victor Eijkhout

► **To cite this version:**

Cédric H. David, David R. Maidment, Guo-Yue Niu, Zong-Liang Yang, Florence Habets, et al..
River network routing on the NHDPlus dataset. *Journal of Hydrometeorology*, 2011, 12, pp.913-934. 10.1175/2011JHM1345.1 . hal-00641713v1

HAL Id: hal-00641713

<https://hal.science/hal-00641713v1>

Submitted on 16 Nov 2011 (v1), last revised 18 Nov 2011 (v2)

HAL is a multi-disciplinary open access archive for the deposit and dissemination of scientific research documents, whether they are published or not. The documents may come from teaching and research institutions in France or abroad, or from public or private research centers.

L'archive ouverte pluridisciplinaire **HAL**, est destinée au dépôt et à la diffusion de documents scientifiques de niveau recherche, publiés ou non, émanant des établissements d'enseignement et de recherche français ou étrangers, des laboratoires publics ou privés.

1 **River network routing on the NHDPlus dataset**

2 Cédric H. David^{1,2}, David R. Maidment², Guo-Yue Niu^{1,3}, Zong-Liang Yang¹, Florence
3 Habets⁴ and Victor Eijkhout⁵

4 1. Department of Geological Sciences, Jackson School of Geosciences, University of
5 Texas at Austin, Austin, Texas, USA.

6 2. Center for Research in Water Resources, University of Texas at Austin, Austin, Texas,
7 USA.

8 3. Biosphere 2, University of Arizona, Tucson, Arizona, USA

9 4. UMR-Sisyphé 7619, CNRS, UPMC, Mines-Paristech, Paris, France.

10 5. Texas Advanced Computing Center, University of Texas at Austin, Austin, Texas,
11 USA.

12 **Key words**

13 RAPID, streamflow, network, matrix, parallel computing, PETSc, TAO

14 **Corresponding author**

15 Cédric H. David

16 Department of Geological Sciences, Jackson School of Geosciences

17 The University of Texas at Austin

18 1 University Station C1160

19 Austin, TX 78712

20 cedric.david@mail.utexas.edu

21 **Abstract**

22 The mapped rivers and streams of the contiguous United States are available in a
23 geographic information system (GIS) dataset called NHDPlus. This hydrographic dataset
24 has about 3 million river and water body reaches along with information on how they are
25 connected into networks. The USGS National Water Information System provides
26 stream flow observations at about 20 thousand gages located on the NHDPlus river
27 network. A river network model called RAPID is developed for the NHDPlus river
28 network whose lateral inflow to the river network is calculated by a land surface model.
29 A matrix-based version of the Muskingum method is developed herein which RAPID
30 uses to calculate flow and volume of water in all reaches of a river network with many
31 thousands of reaches, including at ungaged locations. Gages situated across river basins
32 (not only at basin outlets) are used to automatically optimize the Muskingum parameters
33 and to assess river flow computations; hence allowing the diagnosis of runoff
34 computations provided by land surface models. RAPID is applied to the Guadalupe and
35 San Antonio River Basins in Texas, where flow wave celerities are estimated at multiple
36 locations using 15-minute data and can be reproduced reasonably with RAPID. This
37 river model can be adapted for parallel computing and although the matrix method
38 initially adds a large overhead, river flow results can be obtained faster than with the
39 traditional Muskingum method when using a few processing cores, as demonstrated in a
40 synthetic study using the Upper Mississippi River Basin.

41

42 **1. Introduction**

43 Land surface models (LSMs) have been developed by the atmospheric science
44 community to provide atmospheric models with bottom boundary conditions (water and
45 energy balance) and to serve as the land base for hydrologic modeling. Over the past two
46 decades, overland and subsurface runoff calculations done by LSMs have extensively
47 been used to provide water inflow to river routing models that calculate river discharge
48 [*De Roo, et al.*, 2003; *Habets, et al.*, 1999a; 1999b; 1999c; 2008; *Lohmann, et al.*, 1998a;
49 1998b; 2004; *Maurer, et al.*, 2001; *Oki, et al.*, 2001; *Olivera, et al.*, 2000]. However,
50 river routing within LSMs has traditionally been done using gridded river networks that
51 best fit the computational domain used in LSMs. Today, geographic information system
52 (GIS) hydrographic datasets are increasingly becoming available at the continental scale
53 such as NHDPlus [*USEPA and USGS*, 2007] and the global scale such as HydroSHEDS
54 [*Lehner, et al.*, 2006]. These datasets provide a vector-based representation of the river
55 network using the “blue line” mapped rivers and streams. Furthermore, observations of
56 the river systems are now widely available in databases such as the USGS National Water
57 Information System for the United States in which thousands of gages are available along
58 with their exact location on the NHDPlus river network. Most studies mentioned above –
59 with the exception of Habets et al. [2008] – use a limited number of gages throughout
60 large river basins, often focusing on gages located at river mouths. As the spatial and
61 temporal resolutions of weather and climate models and their underlying land surface
62 models increase, using gages located across basins would help diagnosing the quality of
63 LSM computations. The latest work on general circulation models by the international
64 scientific community, especially by the intergovernmental panel on climate change

65 [Solomon, *et al.*, 2007], opens potential studies of the evolution of water resources with
66 global change. Using mapped streams and water bodies in LSMs could benefit the
67 resulting assessment of the impact of global change in water resources by providing
68 estimation of changes at the “blue line” level. Furthermore, the use of parallel computing
69 is quite common in regional- to global-scale atmospheric and ocean modeling, but
70 comparatively infrequent in modeling of large river networks. Generally, parallel
71 computing can be utilized to either solve problems of increasing size [as done with the
72 ParFlow model: Jones and Woodward, 2001; Kollet and Maxwell, 2006; Kollet, *et al.*,
73 2010] or to decrease computation time [see, for example: Apostolopoulos and
74 Georgakakos, 1997; Larson, *et al.*, 2007; Leopold, *et al.*, 2006; von Bloh, *et al.*, 2010].
75 These two types of approaches to parallel computing are respectively referred to as
76 scalability and speedup of calculations and the work presented herein focuses on the
77 latter. Apostolopoulos and Georgakakos [1997] investigated the speedup of streamflow
78 computations using hydrologic models in river networks as a function of network
79 decomposition and of the computing time ratio between vertical and horizontal water
80 balance calculations. Simple river routing within LSMs being traditionally performed by
81 carrying computations from upstream to downstream, one way to speedup river flow
82 modeling is to use a sequential river routing code to compute independent basins on
83 different processing cores, as done in Leopold *et al.* [2006] and in Larson *et al.* [2007].
84 Such methods allow avoiding inter-processor communication but result in imbalanced
85 computing loads when some basins are much larger than others. Leopold *et al.* [2006]
86 partly addressed load imbalance by using parallel computing for surface water balance,
87 but the river routing part remains sequential. von Blow *et al.* [2010] implemented a

88 routing method in which computations do not have to be carried in order from upstream
89 to downstream, therefore obtaining almost perfect speedup. The work developed herein
90 investigates a way to obtain speedup while retaining traditional upstream-to-downstream
91 computations which are used in most river routing schemes.

92 The present study links a land surface model with a new river network model called
93 RAPID using NHDPlus for the representation of the river network and USGS National
94 Water Information System (NWIS) gages for the optimization of model parameters and
95 the assessment of river flow computations. All models and datasets used herein are
96 available at least for the contiguous United States. The work presented here focuses first
97 on the Guadalupe and San Antonio Basins in Texas (see Figure 1) together covering a
98 surface area of about 26,000 km². These basins have about 5,000 river reaches and their
99 corresponding catchments in the NHDPlus dataset (see Figure 2) out of 3 million for the
100 United States. These two basins are also chosen for study because of significant
101 contributions to surface water flow from groundwater sources, because of a large
102 reservoir, at Canyon Lake, where the impacts of constructed infrastructure on flow
103 dynamics have to be considered, and because these rivers flow out into an estuarine
104 system at San Antonio Bay. A synthetic study of the performance of RAPID in a parallel
105 computing environment is also presented using the Upper Mississippi River Basin (see
106 Figure 3), which has about 180,000 river reaches in NHDPlus and covers an area of about
107 490,000 km².

108 The research presented in this paper aims at answering the following questions: how can
109 a river model be developed for calculation of flow and volume of water in a river network
110 of thousands of “blue-line” river reaches? How can the connectivity information in

111 NHDPlus be used to run a river network model in part of the United States? How can
112 flow at ungaged locations be reconstructed? How can model computations be assessed
113 and optimized based on all available measurements? How can parallel computing be
114 used to speedup upstream-to-downstream computations of river flow within a large river
115 network?

116 First, the development of the RAPID model presented. Then, the modeling framework
117 for calculation of river flow in the Guadalupe and San Antonio River Basins using runoff
118 data from a land surface model is developed, followed by results. Finally, the speedup of
119 RAPID in a parallel computing environment is assessed.

120

121 **2. Model development**

122 The model presented here is named RAPID (Routing Application for Parallel
123 computation of Discharge - <http://www.geo.utexas.edu/scientist/david/rapid.htm>).

124 RAPID is based on the traditional Muskingum method that was first introduced by
125 McCarthy [1938] and has been extensively studied in the literature in the past 70 years.

126 The Muskingum method has two parameters, k and x , respectively a time and a
127 dimensionless parameter. Among the most noteworthy papers related to the Muskingum
128 method, Cunge [1969] showed the Muskingum method is a first-order approximation of
129 the kinematic and diffusive wave equation and proposed a method known as the
130 Muskingum-Cunge method – a second-order approximation of the kinematic and
131 diffusive wave equation – in which the Muskingum parameters are computed based on
132 mean physical characteristics of the river channel and of the flow wave. Koussis [1978]
133 proposed a variable-parameter Muskingum method based on the Muskingum-Cunge
134 method where k varies with the flow but x remains constant on the grounds that the
135 Muskingum method is relatively insensitive to this parameter. Other variable-parameter
136 Muskingum methods allow both k and x to vary [see, for example: *Miller and Cunge*,
137 1975; *Ponce and Yevjevich*, 1978], although these variable-parameter methods fail to
138 conserve mass [*Ponce and Yevjevich*, 1978]. Notable large-scale uses of the variable-
139 parameter Muskingum-Cunge method include Orlandini and Rosso [1998] and Orlandini
140 et al. [2003]. More recently, Todini [2007] developed a mass-conservative variable-
141 parameter Muskingum method known as the Muskingum-Cunge-Todini method.

142 As a first step, the traditional Muskingum method with temporally-constant parameters
143 calculated partly based on the work of Cunge [1969] is used in this study because there

144 are significant challenges to overcome in adapting the Muskingum method for river
145 networks, in efficiently running it within a parallel computing environment and in
146 developing an automated parameter estimation procedure before more sophisticated flow
147 equations are used. However, the physics of flow could be improved with many
148 variations based on the Muskingum method or adapted to the Saint Venant equations.

149 **2.1 Calculation of flow and volume of water in a river network**

150 In a network of thousands of reaches, matrices are needed for network connectivity and
151 flow computation. The backbone of RAPID is a vector-matrix version of the Muskingum
152 method shown in Equation (1) and derived subsequently in this section.

153

$$154 \quad (\mathbf{I} - \mathbf{C}_1 \cdot \mathbf{N}) \cdot \mathbf{Q}(t + \Delta t) = \mathbf{C}_1 \cdot \mathbf{Q}^e(t) + \mathbf{C}_2 \cdot [\mathbf{N} \cdot \mathbf{Q}(t) + \mathbf{Q}^e(t)] + \mathbf{C}_3 \cdot \mathbf{Q}(t) \quad (1)$$

155

156 where t is time and Δt is the river routing time step. The bolded notation is used for
157 vectors and matrices. \mathbf{I} is the identity matrix. \mathbf{N} is the river network matrix. \mathbf{C}_1 , \mathbf{C}_2 and
158 \mathbf{C}_3 are parameter matrices. \mathbf{Q} is a vector of outflows from each reach, and \mathbf{Q}^e is a vector
159 of lateral inflows for each reach. Such a vector-matrix formulation of the Muskingum
160 method has to our knowledge never been previously published.

161 Equation (1) is used for river network routing and can be solved using a linear system
162 solver. The vector-matrix notation provides one flow equation for the entire river
163 network, therefore avoiding spatial iterations. For a river network with m river reaches,
164 all vectors are of size m and all matrices are square of size m . Each element of a vector
165 corresponds to one river reach in the network. For performance purposes, all matrices are

166 stored as sparse matrices (only the non-zero values are recorded). A five-reach, two-node
 167 and two-gage river network is used here to clarify the mathematical formulation of the
 168 river network model and is shown in Figure 4a). The river network is made up of a
 169 combination of river reaches similar to that of Figure 4b). The model formulation is
 170 presented here for a small river network but can be generalized to any size of river
 171 network.

172 \mathbf{Q} is a vector of the outflows Q_j of all reaches of the river network, where j is the index
 173 of a river reach within the network:

174

$$175 \quad \mathbf{Q}(t) = \begin{bmatrix} Q_1(t) \\ Q_2(t) \\ Q_3(t) \\ Q_4(t) \\ Q_5(t) \end{bmatrix} = [Q_j(t)]_{j \in [1,m]} \quad (2)$$

176

177 \mathbf{Q}^e is a vector of flows Q_j^e that are lateral inflows to the river network. Lateral inflows
 178 include runoff, groundwater or any type of forced inflow (outflow at a dam, pumping,
 179 etc.):

180

$$181 \quad \mathbf{Q}^e(t) = [Q_j^e(t)]_{j \in [1,m]} \quad (3)$$

182

183 \mathbf{Q}^e is provided by a land surface model, whose time step is coarser than the river routing
 184 time step. Two assumptions are made in the development of RAPID, one regarding the

185 temporal variability of Q^e and one regarding the location at which Q^e enters the river
 186 network. In this study, the river routing time step is 15 minutes and inflow from land
 187 surface runoff is available every 3 hours. In the derivation of Equation (1), Q^e is
 188 assumed constant (i.e. $Q^e(t + \Delta t) = Q^e(t)$) over all 15-minute river routing time steps
 189 included within a given land surface model 3-hour time step. This partial temporal
 190 uniformity simplifies the river network model formulation, limits the quantity of input
 191 data and facilitates the coupling with land surface models. This assumption is valid at all
 192 times except at the last routing time steps before a new Q^e is made available by the land
 193 surface model. Also, the external inflow Q^e is assumed to enter the network as an
 194 addition to the upstream flow. With these two assumptions, the Muskingum method
 195 applied to reach 5 in Figure 4b) gives the following:

196

$$\begin{aligned}
 Q_5(t + \Delta t) = & C_1 \cdot [Q_3(t + \Delta t) + Q_4(t + \Delta t) + Q^e_5(t)] \\
 & + C_2 \cdot [Q_3(t) + Q_4(t) + Q^e_5(t)] \\
 & + C_3 \cdot Q_5(t)
 \end{aligned} \tag{4}$$

198

199 where C_1 , C_2 and C_3 are the Muskingum parameters that are stated in Equation (6). The
 200 reader should note that these two assumptions are equivalent to using a unit-width lateral
 201 inflow along with a term C_4 as found in available literature [see, for example: *Fread*,
 202 1993; *NERC*, 1975; *Orlandini and Rosso*, 1998; *Ponce*, 1986]. Equation (1) is a
 203 generalization of Equation (4) using a vector-matrix notation.

204 \mathbf{N} is a network connectivity matrix. Berge [1958] proposed the concept of matrices
 205 associated with graphs. This concept can be applied to the river network in Figure 4a) in
 206 order to create the network matrix \mathbf{N} given in Equation (5) in both full and sparse
 207 formats. The network connectivity matrix is a square matrix whose dimension is the total
 208 number of reaches in the network. A value of one is used at row i and column j if reach
 209 j flows into reach i and zero is used everywhere else.

210

$$211 \quad \mathbf{N} = \begin{bmatrix} 0 & 0 & 0 & 0 & 0 \\ 0 & 0 & 0 & 0 & 0 \\ 1 & 1 & 0 & 0 & 0 \\ 0 & 0 & 0 & 0 & 0 \\ 0 & 0 & 1 & 1 & 0 \end{bmatrix} = \begin{bmatrix} & & & & \\ & & & & \\ 1 & 1 & & & \\ & & & & \\ & & & 1 & 1 \end{bmatrix} \quad (5)$$

212

213 The upstream inflow to the network can therefore be computed by multiplying the
 214 network connectivity matrix \mathbf{N} by the vector of outflows \mathbf{Q} . In case of a divergence in
 215 the river network (when going downstream) or in case of a loop, a unique reach (the
 216 major divergence) is used to carry all the upstream flow and the other reaches (minor
 217 divergences) carry only the flow that results from their lateral inflow. This formulation
 218 could be modified to take into account given fractions of flows that separate into different
 219 parts of a divergence if that information is available.

220 \mathbf{C}_1 , \mathbf{C}_2 and \mathbf{C}_3 are diagonal matrices with their diagonal elements being the coefficients
 221 used in the Muskingum method [McCarthy, 1938], respectively C_{1j} , C_{2j} and C_{3j} such
 222 that:

223

$$224 \quad C_{1j} = \frac{\frac{\Delta t}{2} - k_j \cdot x_j}{k_j \cdot (1 - x_j) + \frac{\Delta t}{2}}, \quad C_{2j} = \frac{\frac{\Delta t}{2} + k_j \cdot x_j}{k_j \cdot (1 - x_j) + \frac{\Delta t}{2}}, \quad C_{3j} = \frac{k_j \cdot (1 - x_j) - \frac{\Delta t}{2}}{k_j \cdot (1 - x_j) + \frac{\Delta t}{2}} \quad (6)$$

225

226 where k_j is a storage constant (with dimension of a time) and x_j a dimensionless
227 weighting factor characterizing the relative influence of the inflow and the outflow on the
228 volume of the reach j . The Muskingum method is stable for any $x \in [0, 0.5]$, regardless
229 of the value of k and Δt [Cunge, 1969]. For any j : $C_{1j} + C_{2j} + C_{3j} = 1$.

230 In RAPID, the parameters k and x of the Muskingum method are allowed to differ from
231 one river reach to another, and corresponding vectors are defined in Equation (7):

232

$$233 \quad \mathbf{k} = [k_j]_{j \in [1, m]} \quad , \quad \mathbf{x} = [x_j]_{j \in [1, m]} \quad (7)$$

234

235 The constants defined in Equation (6) are used as the diagonal elements of the matrices
236 \mathbf{C}_1 , \mathbf{C}_2 and \mathbf{C}_3 . Equation (8) shows an example for \mathbf{C}_1 . \mathbf{C}_2 and \mathbf{C}_3 are treated similarly.

237

$$238 \quad \mathbf{C}_1 = \begin{bmatrix} C_{1_1} & & & & \\ & C_{1_2} & & & \\ & & C_{1_3} & & \\ & & & C_{1_4} & \\ & & & & C_{1_5} \end{bmatrix} \quad (8)$$

239

240 The sum $\mathbf{C}_1 + \mathbf{C}_2 + \mathbf{C}_3$ equals the identity matrix.

241 The calculation of the volume of water in a given reach can be needed for coupling with
242 groundwater models. Here, the first order, explicit, forward Euler method is applied to
243 the continuity equation to calculate the volume of water in each river reach of the
244 network, as shown in Equation (9) where the first, second and third terms of the right-
245 hand-side are the volume of water that respectively were in the river reach, flowed into
246 the reach, and discharged from the reach:

247

$$248 \quad \mathbf{V}(t + \Delta t) = \mathbf{V}(t) + [\mathbf{N} \cdot \mathbf{Q}(t) + \mathbf{Q}^e(t)] \cdot \Delta t - \mathbf{Q}(t) \cdot \Delta t \quad (9)$$

249

250 where \mathbf{V} is a vector of the volume of water V_j in each river reach j :

251

$$252 \quad \mathbf{V}(t) = [V_j(t)]_{j \in \{1, m\}} \quad (10)$$

253

254 Details on the massively-parallel implementation of the matrix-based Muskingum
255 method presented in this section, and of the automated parameter estimation presented in
256 the section below are given in Appendix A.

257 **2.2 Parameter estimation**

258 In order to estimate the parameters \mathbf{k} and \mathbf{x} to be used in RAPID, an inverse method is
259 developed. The principle of an inverse method is to optimize the parameters of a model
260 so that the outputs of the model approach observations. A cost function reflecting the

261 difference between model calculations and observations is needed to assess the quality of
 262 a set of model parameters. The best set of parameters is chosen as the set that minimizes
 263 the cost function, and is determined through optimization. A square-error cost function
 264 ϕ is chosen:

265

$$266 \quad \phi(\mathbf{k}, \mathbf{x}) = \sum_{t=t_o}^{t=t_f} \left[\left(\frac{\bar{\mathbf{Q}}(t) - \mathbf{Q}^g(t)}{f} \right)^T \cdot \mathbf{G} \cdot \left(\frac{\bar{\mathbf{Q}}(t) - \mathbf{Q}^g(t)}{f} \right) \right] \quad (11)$$

267

268 where the summation is made daily. The T in exponent is for vector transpose. t_o and
 269 t_f are respectively the first day and last day used for the calculation of ϕ . The model
 270 parameter vectors \mathbf{k} and \mathbf{x} are kept constant within the temporal interval $[t_o, t_f]$, and the
 271 cost function is calculated several times with different sets of parameters during the
 272 optimization procedure. f is a scalar that allows ϕ to be on the order of magnitude of
 273 10^1 which is helpful for automated optimization procedures. $\bar{\mathbf{Q}}(t)$ is the daily-average
 274 outflow vector, calculated based on the mean of all routing time steps in a given day.
 275 $\mathbf{Q}^g(t)$ is a vector with the total number of river reaches for dimension, with the daily
 276 value observed $Q_j^g(t)$ corresponding to reach j where gage measurements are available,
 277 and zero where no gage is available. \mathbf{G} is a sparse diagonal matrix that allows the dot-
 278 product to survive only where gages are available, so that \mathbf{G} has a value of one on the

279 diagonal element of index j if a gage is available on reach j and zero everywhere else.

280 Using the example network given in Figure 4a), \mathbf{G} and $\mathbf{Q}^g(t)$ take the following form:

281

$$282 \quad \mathbf{G} = \begin{bmatrix} & & & \\ & & & \\ & & 1 & \\ & & & \\ & & & & 1 \end{bmatrix}, \quad \mathbf{Q}^g(t) = \begin{bmatrix} 0 \\ 0 \\ Q_{5,0g}^g(t) \\ 0 \\ Q_{5,0g}^g(t) \end{bmatrix} \quad (12)$$

283

284 According to Fread [1993], $x \in [0.1; 0.3]$ in most streams. By analogy with the kinematic

285 wave equation, Cunge [1969] showed that the parameter k of the Muskingum method is

286 the travel time of a flow wave through a river reach. For a given river reach j of length

287 L_j where a flow wave of celerity c_j travels, k_j is obtained by dividing the length by the

288 celerity of the wave, as shown in Equation (13):

289

$$290 \quad k_j = \frac{L_j}{c_j} \quad (13)$$

291

292 Although the routing model defined by Equation (1) allows for variability of the

293 parameters (k_j, x_j) on a reach-to-reach basis, attempting to automatically estimate model

294 parameters independently for all the reaches of a basin would be a costly undertaking.

295 Therefore, the search for optimal parameters is limited to determining two multiplying

296 factors λ_k and λ_x such that:

297

298
$$k_j = \lambda_k \cdot \frac{L_j}{c_j} \quad , \quad x_j = \lambda_x \cdot 0.1 \quad (14)$$

299

300 To minimize the influence of the initial guess on the optimization procedure, three
301 different initial guesses for (λ_k, λ_x) are used. Out of the three corresponding optimal
302 (λ_k, λ_x) obtained, only the one couple leading to the minimum value of the cost function
303 ϕ is kept. Therefore, the optimization procedure leads to only one optimal couple
304 (λ_k, λ_x) for a given basin in the network. Note that – as a first step – \mathbf{x} is here constant
305 over a given basin on the grounds that the Muskingum method is relatively insensitive to
306 this parameter [Koussis, 1978]. Some data available in NHDPlus (such as mean flow,
307 mean velocity, slope, etc.) associated with available formulations for \mathbf{x} [for example:
308 Cunge, 1969; Orlandini and Rosso, 1998] could be used to improve the proposed
309 method.

310 **3. Application**

311 RAPID is designed to handle large routing problems. Given a river network and
312 connectivity information as well as lateral inflow to the river network, RAPID can run on
313 any river network. In this study, a framework for computation of river flow in the
314 Guadalupe and San Antonio River Basins is developed that uses a one-way modeling
315 framework with an atmospheric dataset, a land surface model and RAPID as the river
316 model. This section presents how the Guadalupe and San Antonio River Basins are
317 described in the NHDPlus dataset, how a land surface model is used to provide lateral
318 inflow to the river network, and how the meteorological forcing is prepared.

319 **3.1. RAPID used on NHDPlus**

320 There are a total of 5175 river reaches with known direction and connectivity within the
321 NHDPlus description of the Guadalupe and San Antonio river basins (as shown in Figure
322 2). These 5175 reaches have an average length of 3.00 km and the average catchment
323 defined around them is 5.11 km² in area; all are used for this study. Details on the fields
324 used in the NHDPlus dataset including the unique identifier COMID used for all river
325 reaches and their corresponding catchments; and on how NHDPlus is used with RAPID
326 are given in Appendix B. In this study, the vector of outflows in all river reaches \mathbf{Q} was
327 arbitrarily initialized to the uniform value of 0 m³s⁻¹ prior to running RAPID.

328 **3.2. Land surface model and coupling with RAPID**

329 Within this study, the core physical model governing the one-dimensional vertical fluxes
330 of energy and moisture is the Community Noah Land Surface Model with Multi-Physics
331 Options, hereafter referred to as Noah-MP [Niu, *et al.*, 2010]. Noah-MP offers multiple
332 options for choosing the modeling of certain physical phenomena. In this study, the soil

333 moisture factor for stomatal resistance is of “Noah type” [Niu, et al., 2010] and the runoff
334 scheme is from “SIMGM” [Niu, et al., 2007]. The soil column is 2 meter deep, below
335 which is an unconfined aquifer. In order to represent the characteristics of the structural
336 soil over the model domain, the saturated hydraulic conductivity, which is determined by
337 the soil texture data, is enlarged by factor of ten (through calibration). The soil
338 hydrology of Noah (soil moisture) is run at an hourly time step and runoff data are
339 produced every three hours. In this study, the state variables of Noah were initialized
340 through a spin-up method.

341 Noah-MP calculates the amount of water that runs off on and below the land surface.
342 This quantity is used to provide RAPID with the water inflow from outside of the river
343 network. David et al. [2009] presented a coupling technique using a hydrologically
344 enhanced version of the Noah LSM called Noah-distributed [Gochis and Chen, 2003]
345 that allows physically-based modeling of the horizontal movement of surface and
346 subsurface water from the land surface to a river reach. In interest of a simpler coupling
347 scheme, the work of David et al. [2009] has been modified. In this study, a flux coupler
348 between Noah and RAPID is developed using the catchments available in the NHDPlus
349 dataset.

350 The NHDPlus catchments contributing runoff to each river reach were determined as part
351 of the NHDPlus development using a digital elevation model and its associated flow
352 accumulation and flow direction grids. These grids have a native resolution of 30 m.
353 The map of catchments is available in NHDPlus in both gridded (at 30-m resolution) and
354 vector formats in a shapefile. Running a land surface model at a 30-m resolution is very
355 resource demanding. Therefore, a coarser resolution of 900 m cell size is chosen. The

356 shapefile of NHDPlus catchment boundaries is converted to a grid of size 900 m. Within
357 this conversion process, the accuracy of the boundaries of the catchments is lowered but
358 the catchment boundaries are reasonably respected and the computational cost of the land
359 surface model calculations is reasonable. For each 3-hour output of the Noah model,
360 surface and subsurface runoff data is superimposed onto the catchment grid, and all
361 runoff that corresponds to the catchment of each river reach is summed and used as the
362 water inflow to the river reach. Figure 5 shows the principle of the flux coupler in which
363 the 900-m runoff data generated by the Noah model is superposed to the 900-m map of
364 NHDPlus catchment COMIDs to determine the lateral inflow for NHDPlus reaches used
365 by RAPID.

366 Therefore, no horizontal routing is used between the land surface and the river network in
367 the proposed scheme. This differs from some other models that use runoff from a one-
368 dimensional model to force a river routing model. For instance, the two dimensional
369 wave equation is used in Gochis and Chen [2003] or the linear reservoir equation is used
370 in Ledoux et al. [1989].

371 The coupling method used here can be adapted to any land surface model that computes
372 surface and subsurface runoff on a grid. This coupling technique is automated in a
373 Fortran program.

374 **3.3. Meteorological forcing**

375 Land surface models need meteorological forcing in order to compute the water and the
376 energy balance at the surface. The Noah LSM requires seven meteorological parameters:
377 precipitation, specific humidity, air temperature, air pressure, wind speed, downward
378 shortwave and downward longwave radiation. Hourly precipitation is obtained from

379 NEXRAD and downscaled from its original resolution (4.763 km) to 900 m using the
380 method developed in Guan et al. [2009]. All other meteorological parameters are
381 downloaded from the 3-hourly North American Regional Reanalysis (NARR) and
382 converted from its original resolution (32.463 km) to 900 m using a simple triangle-base
383 linear interpolation. All meteorological data are prepared for four years (01 January 2004
384 – 31 December 2007).
385
386

387 **4. Calibration and results for the Guadalupe and San Antonio River Basins**

388 The framework for computation of river flow that is developed in the previous section is
389 used to calculate river flow in all 5175 river reaches of the Guadalupe and San Antonio
390 River Basins for four years (01 January 2004 – 31 December 2007). In this section, flow
391 wave celerities in several sub-basins are estimated from measurements, the model
392 parameters used in RAPID are presented, and flows computed are compared to observed
393 flows. Issues related to the time step used in RAPID and to the simulated wave celerities
394 are also presented.

395 **4.1. Estimation of wave celerities**

396 The USGS Instantaneous Data Archive (<http://ida.water.usgs.gov/ida/>) provides 15-
397 minute flow data that can be used to determine the flow wave celerity. Data at fifteen
398 gaging stations within the two basins studied are obtained from IDA over two time
399 periods (01 January 2004 – 30 June 2004 and for 01 January 2007 – 30 June 2007). The
400 maximum lagged cross-correlation between hydrographs at two consecutive gaging
401 stations is used to determine the flow wave celerity. The lagged cross-correlation ρ is a
402 measure of similarity between two wave forms as a function of a lag time τ_{lag} applied to
403 one of them, as shown in Equation (15).

404

405
$$\rho = \frac{\sum(Q^a(t) - \bar{Q}^a) \cdot (Q^b(t + \tau_{lag}) - \bar{Q}^b)}{\sqrt{\sum(Q^a(t) - \bar{Q}^a)^2 \cdot \sum(Q^b(t + \tau_{lag}) - \bar{Q}^b)^2}} \quad (15)$$

406

407 where Q^a and Q^b are the flows measured at the upstream and downstream station,
408 respectively; and the summation is here made every 15 minutes for 6 months. Figure 6
409 shows the correlation as a function of increasing lag time between three different sets of
410 consecutive gaging stations. The lag time giving the maximum correlation is taken as the
411 travel time τ_{travel} for the flow wave between the two stations. The travel times are
412 estimated for eleven sets of two stations and are shown on Table 1. Travel times of 0 s
413 are reported at two stations, where the flow wave is probably too fast to be captured by
414 15-minute measurements. The wave celerity c is then computed using Equation (16)

415

$$416 \quad c = \frac{d}{\tau_{travel}} \quad (16)$$

417

418 where d is the distance between two stations. The NHDPlus Flow Table Navigator Tool
419 (<http://www.horizon-systems.com/nhdplus/tools.php>) is used to estimate the curvilinear
420 distance between two stations along the NHDPlus river network that are shown on Table
421 1. The wave celerity has been estimated for eleven sub-basins within the Guadalupe and
422 San Antonio river basins. Table 2 shows the values that are obtained for the two time
423 periods considered, as well as their average. Figure 7 shows the corresponding sub-
424 basins as well as the locations of all gaging stations.

425 **4.2. Parameters used in RAPID**

426 RAPID needs two vectors of parameters \mathbf{k} and \mathbf{x} that can either be determined using
427 physically-based equations, through optimization, or a combination of both. In this
428 study, daily stream flow data are obtained from the USGS National Water Information

429 System (<http://waterdata.usgs.gov/nwis>) in order to use the built-in parameter estimation.
 430 Within the Guadalupe and San Antonio river basins, NWIS has 74 gages that measure
 431 flow, 36 of them having full records of daily measurements the four years studied (01
 432 January 2004 – 31 December 2007). These 36 stations are used for parameter estimation.
 433 Four sets of model parameters – denoted by the superscripts α, β, γ and δ – are used in
 434 this study. These sets of parameters are all based on Equation (14) which is used with a
 435 uniform wave celerity of $c^0 = 1km \cdot h^{-1} = 0.28m \cdot s^{-1}$ throughout the basin or with the
 436 celerities c_j determined based on the IDA lagged cross-correlation study.
 437 The first set, $(\mathbf{k}^\alpha, \mathbf{x}^\alpha)$ is obtained from parameter estimation shown in Equation (11) using
 438 the uniform wave celerity $c^0 = 0.28m \cdot s^{-1}$ and the resulting values of the two multiplying
 439 factors λ_k and λ_x of Equation (14) are:

440

$$\begin{aligned}
 441 \quad k_j^\alpha &= \lambda_k^\alpha \cdot \frac{L_j}{c^0} \quad , \quad x_j^\alpha = \lambda_x^\alpha \cdot 0.1 \\
 \lambda_k^\alpha &= 0.131042 \quad , \quad \lambda_x^\alpha = 2.58128
 \end{aligned}
 \tag{17}$$

442

443 The parameters $(\mathbf{k}^\beta, \mathbf{x}^\beta)$ are determined without optimization using the celerities
 444 c_j determined based on the IDA lagged cross-correlation study and set to:

445

$$\begin{aligned}
 446 \quad k_j^\beta &= \lambda_k^\beta \cdot \frac{L_j}{c_j} \quad , \quad x_j^\beta = \lambda_x^\beta \cdot 0.1 \\
 \lambda_k^\beta &= 1 \quad , \quad \lambda_x^\beta = 1
 \end{aligned}
 \tag{18}$$

447

448 The third set of parameters ($\mathbf{k}^\gamma, \mathbf{x}^\gamma$) is obtained through optimization using the celerities
449 c_j determined based on the IDA lagged cross-correlation study and the resulting values
450 are:

451

$$\begin{aligned} 452 \quad k_j^\gamma &= \lambda_k^\gamma \cdot \frac{L_j}{c_j} \quad , \quad x_j^\gamma = \lambda_x^\gamma \cdot 0.1 & (19) \\ \lambda_k^\gamma &= 0.617188 \quad , \quad \lambda_x^\gamma = 1.95898 \end{aligned}$$

453

454 The optimization converges to a value of \mathbf{k} that is 38% smaller than that estimated with
455 the IDA lagged cross-correlation, suggesting that a faster flow wave in the river network
456 produces better flow calculations. In the present study, routing on the land surface from
457 the catchment to its corresponding reach is not modeled. Therefore, one would expect
458 that the optimized flow celerity in the river network would be slower than that estimated
459 from river flow observations, which is not the case here. This suggests that runoff is
460 either produced too slowly or too far upstream of each gage; maybe because runoff in
461 land surface models is often calibrated based on a lumped value at the downstream gage
462 of a basin, as was done here with Noah-MP. Further details on the quality of runoff
463 simulations are given in Section 4.4.

464 The fourth set of parameters ($\mathbf{k}^\delta, \mathbf{x}^\delta$) is determined for a better match of celerity
465 calculations, as explained later in this paper.

466 **4.3. Time step of RAPID simulation**

467 Cunge [1969] showed that the Muskingum method is stable for any $x \in [0, 0.5]$ and that
468 the wave celerity computed by the Muskingum method approaches the theoretical wave
469 celerity of the kinematic wave equation if the time step of the river routing equals the
470 travel time of the wave (for $x = 0.5$), as shown in Equation (20):

471

$$472 \quad \forall j \in [1, m] \quad c_j \approx \frac{L_j}{\Delta t} \quad (20)$$

473

474 However, both the celerity of flow and the length of river reaches vary along the network;
475 and the model formulation of RAPID allows for only one unique value of the time step
476 Δt be chosen. In the Guadalupe and San Antonio River Basins, the mean length is 3 km
477 and the median length is 2.4 km. The probability density function and the cumulative
478 density functions for the lengths of river reaches are shown in Figure 8. The celerities
479 estimated earlier are on the order of $c = 2.5m \cdot s^{-1}$. Using the median value of the reach
480 length along with $c = 2.5m \cdot s^{-1}$, Equation (20) gives $\Delta t = 960s$. In order to have an
481 integer conversion between the river routing time step and the land surface model time
482 step (3 hours), a value of $\Delta t = 900s = 15 \text{ min}$ is chosen.

483 **4.4. Analysis of the quality of river flow computation**

484 For various model simulations, the average and the root mean square error (RMSE) of
485 computed flow rate are calculated using daily data and are given in Table 3. The Nash
486 efficiency [*Nash and Sutcliffe*, 1970] is bounded by the interval $]-\infty, 1]$ and gives an
487 estimate of the quality of modeled river flow computations when compared to

488 observations; and is also given in Table 3. An efficiency of 1 corresponds to a perfect
489 model and 0 corresponds to a model producing the mean of observations. The results
490 shown for a lumped model correspond to when runoff from Noah is accumulated at the
491 gage directly without any routing. The average values of flow in RAPID simulations are
492 tied to the amount of runoff water calculated by the Noah LSM and the bias generated by
493 the land surface model cannot be fixed by RAPID. However, the internal connectivity of
494 the NHDPlus river network is well translated in RAPID and mass is conserved within
495 RAPID since the flow rates in the lumped simulation and in all four simulations of
496 RAPID are the same. Figure 9 shows the ratio between observed and lumped stream
497 flow at 17 gages located across the Guadalupe and San Antonio River Basins. This ratio
498 is around unity downstream of the Guadalupe and San Antonio Rivers, but is greater than
499 7 upstream; suggesting that runoff is most likely overestimated at the center of the basin.
500 Additionally, runoff is largely underestimated at two stations just downstream of the
501 outcrop area of the Edwards Aquifer: the Comal River at New Braunfels and the San
502 Marcos River at San Marcos. These stations measure large average stream flow
503 (respectively $10.59 \text{ m}^3/\text{s}$ and $5.9 \text{ m}^3/\text{s}$) although draining a relatively small area
504 (respectively 336 km^2 and 129 km^2), and are actually two of the largest springs in Texas.
505 These flows are much larger than the lumped runoff (respectively $0.67 \text{ m}^3/\text{s}$ and 0.26
506 m^3/s), which is expected because the modeling framework presented herein does not
507 not explicitly simulate aquifers.
508 However, the RAPID simulations $(\mathbf{k}^a, \mathbf{x}^a)$, $(\mathbf{k}^b, \mathbf{x}^b)$ and $(\mathbf{k}^\gamma, \mathbf{x}^\gamma)$ lead to a smaller RMSE
509 and a higher Nash Efficiency than the lumped runoff. This shows that an explicit river

510 routing scheme with carefully-chosen parameters allows obtaining better stream flow
511 calculations than a simple lumped runoff scheme, as expected.

512 Within the different RAPID simulations, the set of parameters $(\mathbf{k}^\gamma, \mathbf{x}^\gamma)$ gives the best
513 results for RMSE and Nash efficiency, followed by $(\mathbf{k}^\beta, \mathbf{x}^\beta)$, $(\mathbf{k}^\alpha, \mathbf{x}^\alpha)$ and $(\mathbf{k}^\delta, \mathbf{x}^\delta)$.

514 Therefore, a greater spatial variability in the values of k contributes to the quality of
515 model results, and the built-in optimization in RAPID further enhances these model
516 results. An example hydrograph for the Guadalupe River near Victoria TX is shown in
517 Figure 10, and is computed using $(\mathbf{k}^\gamma, \mathbf{x}^\gamma)$.

518 **4.5. Comparison between estimated and computed wave celerities**

519 In order to assess the capacity of the modeling framework to reproduce surface flow
520 dynamics, the celerity of the flow wave in outputs from RAPID are computed. Fifteen-
521 minute river flow is computed with RAPID, and the lagged cross-correlation presented
522 earlier is used to calculate the wave celerity within the RAPID simulation. Table 2 shows
523 the celerities that are computed from RAPID outputs. In the first three sets of model
524 parameters used, the wave celerities simulated in RAPID are greater than those observed.

525 One can also notice that even for $(\mathbf{k}^\beta, \mathbf{x}^\beta)$, the model-simulated celerities are different
526 than the observed celerities which are used to determine the vector \mathbf{k}^β itself. This was
527 predicted by Cunge [1969] who showed that the difference between the celerity of the
528 kinematic wave equation and that computed using the Muskingum method is a function
529 of both x and the quotient $\Delta t/L_j$. Only the specific values $x = 0.5$ and Δt verifying
530 $\Delta t/L_j = c_j$ allow obtaining the same celerity. Furthermore, the work herein is done in a

531 river network, and the celerity estimated between two points does not correspond only to
 532 the main river stem but rather to a combination of all river reaches present in the network
 533 in between the two points. The ratio of the average celerities from RAPID using
 534 $(\mathbf{k}^{\beta}, \mathbf{x}^{\beta})$ over the average observed celerities is 1.54. As a final experiment, a new set of
 535 parameters $(\mathbf{k}^{\delta}, \mathbf{x}^{\delta})$ is created to account for the faster waves in RAPID.

536

$$\begin{aligned}
 537 \quad k_j^{\delta} &= \lambda_k^{\delta} \cdot \frac{L_j}{c_j} \quad , \quad x_j^{\delta} = \lambda_x^{\delta} \cdot 0.1 & (21) \\
 \lambda_k^{\delta} &= 1.54 \quad , \quad \lambda_x^{\delta} = 1
 \end{aligned}$$

538

539 Table 2 shows that the parameters $(\mathbf{k}^{\delta}, \mathbf{x}^{\delta})$ allow for wave celerities that are closer to the
 540 observed ones than the celerities obtained with the other sets of parameters. The average
 541 flow wave celerity over the 11 calculations in RAPID is within 3% of that estimated with
 542 IDA flows. Unfortunately, these closer wave celerities also lead to a decrease in the
 543 quality of RMSE and Nash Efficiency. Therefore, model celerities closer to celerities
 544 estimated from observations can be obtained, but generally deteriorate other statistics of
 545 calculations. Again, this might be due to runoff being produced too slowly or too far
 546 upstream of each gage.

547 **4.6 Statistical Significance**

548 Changes in the routing procedure – i.e. no routing or routing using various RAPID
 549 parameters – lead to various changes in the values of efficiency and RMSE, as shown in
 550 Section 4.2. The statistical significance of the changes can be assessed in order to

551 determine whether or not various routing experiments are effective. For two different
552 routing procedures used, the efficiency (respectively RMSE) at one gage can be
553 compared to the efficiency (respectively RMSE) at the same gage, although variability of
554 efficiency (respectively RMSE) between independent gages can be large. Therefore,
555 there is a logical pairing of efficiency and RMSE calculated at a given gage between two
556 experiments and hence matched pair tests are appropriate to assess the statistical
557 significance. Several common options are available for matched pair tests (with
558 increasing level of complexity): the sign test, the Wilcoxon signed-ranked test [*Wilcoxon*,
559 1945] and the paired t-test. The sign test has no assumption on the shape of probability
560 distributions of samples used but is quite simple since only the sign of differences
561 between two paired samples is accounted for. The Wilcoxon signed-ranks test
562 incorporates the magnitude of differences between paired samples under the assumption
563 that differences between pairs are symmetrically distributed. The paired t-test may be
564 used when the differences between pairs are known to be normally distributed. The
565 assumption of the Wilcoxon signed-ranks test (symmetry) is not as restrictive as that of
566 the paired t-test (normality). In case where small sample sizes are used – as done in this
567 study – testing for symmetry or normality may not be meaningful. Additionally,
568 violations of the symmetry assumption in the Wilcoxon signed-ranks test have minimal
569 influence on the corresponding p-values [*Helsel and Hirsch*, 2002]. These two reasons
570 motivate the use of the Wilcoxon signed-ranks test in the study herein. The null
571 hypothesis H_0 for this test is that the median of differences between two populations is
572 zero. The purpose of changes in the routing procedure being to improve results by

573 increasing the efficiency and decreasing the RMSE, alternate hypotheses can assume that
574 one population tends to be generally either larger (H_1) or smaller (H_2) than the other.
575 Therefore, p-values corresponding to one-sided tests are used in this study. Low
576 significance levels mean that H_0 is unlikely, hence that a significant change is observed.
577 The Wilcoxon signed-ranks test sorts pairs with nonzero difference based on the absolute
578 value of the differences and sums all positive (respectively negative) ranks in a variable
579 named W^+ (respectively W^-). The corresponding p-values vary with the number of
580 nonzero differences and with the value of W^+ and W^- . Fortran programs were created to
581 compute the exact value of the test statistic (not using a large-sample approximation) as
582 well as the corresponding p-values. Table 4 shows the results of the Wilcoxon signed-
583 ranks test for both efficiency and RMSE and for several paired experiments using two
584 different routing procedures. The same 15 stations named on Figure 7 and used in Table
585 3 serve here for statistical significance assessment and the corresponding 15 values of
586 efficiency and of RMSE are utilized as sample values.
587 Several conclusions can be drawn from Table 4. First, the Wilcoxon signed-ranks tests
588 comparing results obtained by RAPID with parameters α , β and γ to a lumped runoff
589 approach show that the null hypothesis can be rejected for a one-sided test at a 10% level
590 of significance in all cases, except for the efficiency between RAPID with β parameters
591 and a lumped approach at a 13% level of significance. All these tests validate that the
592 improvements mentioned in Section 4.2 (increased efficiency and decreased RMSE) are
593 statistically significant and confirm that an explicit river routing scheme allows obtaining
594 better stream flow calculations than a simple lumped runoff scheme, as expected.

595 Second, comparisons between RAPID using α and γ parameters show that sub-basin
596 variability in wave celerities is advantageous to a spatially uniform wave celerity
597 approach at a 19% level of significance for efficiency and at a 7% level for RMSE.
598 Third, comparisons between RAPID using γ and δ parameters confirms that wave
599 celerities close to those determined from observations deteriorate results at a 3% level of
600 significance for both efficiency and RMSE. Finally, one cannot conclude on the
601 statistical significance of the comparison between RAPID using β and γ parameters
602 concerning the improvement of optimization procedure. However, since RAPID
603 using γ parameters produce better average values than RAPID using β parameters and
604 since the statistical significance of RAPID using γ parameters compared to a lumped
605 approach is better than that of RAPID using β parameters compared to lumped approach,
606 the optimization can still considered advantageous.
607
608

609 **5. Synthetic study of the Upper Mississippi River Basin, speedup of parallel**
610 **computations**

611 Through the use of mathematical and optimization libraries that run in a parallel
612 computing environment, RAPID can be applied on several processing cores. The work
613 presented above focuses on the Guadalupe and San Antonio River basins together
614 forming a river network with 5,175 river and water body reaches, which size do not
615 justify the use of parallel computing. However, all the tools and datasets used are
616 available for the Contiguous United States where the NHDPlus dataset has about 3
617 million reaches. Adapting the proposed framework to simultaneously compute flow and
618 volume of water in all mapped water bodies of the contiguous United States would
619 require solving matrix equations of size 3 million. For such a large scientific problem,
620 parallel computing can be helpful if speedup can be achieved, i.e. if increasing the
621 number of processing cores decreases the total computing time.

622 **5.1 Synthetic study used for assessment of parallel performance**

623 As a proof of concept, the evaluation of the parallel computing capabilities of RAPID is
624 presented here using the Upper Mississippi River Basin (shown on Figure 3) which has
625 182,240 river and water body reaches available as Region 07 in the NHDPlus dataset.
626 The number of computational elements for the Upper Mississippi River Basin is about 35
627 times larger than the combination of the Guadalupe and San Antonio River Basins, and
628 about 16 times smaller than the entire Contiguous United States. The river network of
629 the Upper Mississippi River Basin is fully interconnected, all water eventually flowing to
630 a unique outlet.

631 In order to assess the performance of RAPID, the same problem consisting in the
632 computation of river flow in all reaches of the Upper Mississippi River Basin, over 100
633 days, at a 900-second time step is solved for all results reported in Section 5.3. For this
634 performance study, the runoff data symbolized by vector \mathbf{Q}^e in Equation (1) are
635 synthetically generated and set to 1 m^3 every 3 hours for all reaches and all time steps
636 and the vectors of parameters \mathbf{k} and \mathbf{x} are temporally and spatially uniform as shown in
637 Equation (22):

638

$$639 \quad k_j = \frac{L_j}{2.5m \cdot s^{-1}} \quad , \quad x_j = 0.3 \quad (22)$$

640

641 **5.2 Basics of solving a linear system on computers**

642 Numerically solving a linear system is typically an iterative process mainly involving
643 two-steps at each iteration: preconditioning followed by applying a linear solver.
644 Preconditioning is a procedure that transforms a given linear system through matrix
645 multiplication into one that is more easily solved by linear solvers, hence decreasing the
646 total number of iterations to find the solution and saving time. If the linear system is
647 triangular, preconditioning is sufficient to solve the problem, and a linear solver is not
648 needed. In a parallel computing environment, a matrix is separated into diagonal and off-
649 diagonal blocks, each processing core being assigned one diagonal block and its adjacent
650 off-diagonal block. Solving a linear system in parallel is made using blocks and parallel
651 preconditioning is determined based on elements in the diagonal blocks. Preconditioning
652 is sufficient to solve a given parallel linear system if the system is diagonal by blocks –

653 i.e. all off-diagonal blocks are empty – and if each diagonal block is triangular; in most
654 other cases iterations of preconditioning and applying a linear solver are needed.

655 **5.3 Parallel speedup of the synthetic study**

656 For comparison purposes, the traditional Muskingum method was also implemented in
657 RAPID in order to assess the performance of the matrix-based Muskingum method
658 developed herein. Figure 11 shows a comparison of computing time between the
659 traditional Muskingum method shown in Equation (4) and applied consecutively from
660 upstream to downstream and the Matrix-based Muskingum method used in RAPID.
661 Only one processor is used for all results in Figure 11 but the computation method
662 differs. The matrix $\mathbf{I} - \mathbf{C}_1 \cdot \mathbf{N}$ being triangular (see Appendix B), solving the linear
663 system of Equation (1) can be limited to matrix preconditioning if using only one
664 processing core. In a parallel computing environment, $\mathbf{I} - \mathbf{C}_1 \cdot \mathbf{N}$ is separated in blocks,
665 each diagonal block corresponding to a sub-basin. With several processing cores, matrix
666 preconditioning would be sufficient to solve Equation (1) if $\mathbf{I} - \mathbf{C}_1 \cdot \mathbf{N}$ could be made
667 diagonal by blocks, each diagonal block being a triangular matrix. In a river network that
668 is fully interconnected such as that of the Upper Mississippi River Basin $\mathbf{I} - \mathbf{C}_1 \cdot \mathbf{N}$
669 cannot be made diagonal by blocks because the connectivity between adjacent sub-basins
670 would always appear as an element in an off-diagonal block matrix (cf. Equation (23))
671 when i and j are connected but belong to different sub-basins). This limitation would
672 not apply if one was to compute the Mississippi River basin on one (or on one set of)
673 processing core(s) and the Colorado River Basin on another (or on another set of)
674 processing core(s) for example. Therefore, when solving Equation (1) on several

675 processing cores for the Upper Mississippi River Basin, preconditioning is not sufficient
676 and iterative methods need be used. An iterative method implies several computations
677 including preconditioning, matrix-vector multiplication and calculation of residual norm
678 at each iteration.

679 On one processing core, solving the matrix-based Muskingum method with
680 preconditioning only is about twice as long as solving the traditional Muskingum method,
681 as shown in Figure 11. This extra time can be explained because the computation of the
682 right-hand-side of Equation (1) is approximately as expensive as solving the traditional
683 Muskingum method and approximately as expensive as preconditioning. However, the
684 computation of the right-hand-side is done only once per time step regardless of the
685 number of iterations if using an iterative linear solver and scales very well because all
686 operations require no communication except for the product $\mathbf{N} \cdot \mathbf{Q}$ which involves little
687 communication. Figure 11 also shows the computing time when using an iterative solver.
688 The sole purpose of the first iteration in an iterative solver is to determine an initial
689 residual error that is to be used as a criterion for convergence in following iterations.
690 This first iteration mainly involves preconditioning and calculation of a residual norm.
691 On one processing core only, the second iteration converges because preconditioning is
692 sufficient. The two iterations and calculations of norms explain the doubling of
693 computing time between preconditioning only and an iterative solver on one unique
694 processing core that is shown in Figure 11. Overall, the overhead created by an iterative
695 solver over the traditional Muskingum method is about a factor of four. Again, both
696 preconditioning and calculation of residual norms scale well although the latter can be
697 limited by communications. Therefore, the main issue with using a matrix method is the

698 number of iterations needed before the iterative solver converges because all other
699 overhead dissipates with an increasing number of processing cores used. Surprisingly,
700 the number of iterations needed for the iterative solver to converge increases much less
701 quickly than the number of processing cores used, hence allowing to gain total
702 computation time with increased number of processing cores and to produce results faster
703 than the traditional Muskingum method as shown on Figure 12. This suggests that even
704 in a basin where all river reaches are interdependent, some upstream and downstream
705 sub-basins can be computed separately in an iterative scheme given that they are distant
706 enough from each other. The physical explanation is that flow waves are not fast enough
707 to travel across the entire basin within one 15-minute time step. This de-coupling of
708 computations could not be achieved by using the traditional version of the Muskingum
709 method, since computations are not iterative and have to be performed going from
710 upstream to downstream. Figure 12 shows that the total computing time with an iterative
711 matrix solver on 16 processing cores is almost a third of the time needed by the
712 traditional Muskingum method and keeps decreasing further with more processing cores.
713 However, as the number of cores increase, the relative importance of the computation of
714 residual norms within the iterative solver increases up to taking almost half of the solving
715 time, as shown in Figure 12. This limitation will most likely disappear as computer
716 technology advances and communication time decreases. One should note that the output
717 files match on a byte-to-byte basis and hence model computations are strictly the same
718 regardless of the method used; i.e. traditional Muskingum method or Matrix-based
719 Muskingum method, iterative or not. This strict similarity between output files and the
720 slow increase in iterations are also verified for the study of the Guadalupe and San

721 Antonio River Basins presented above; hence the use of synthetic data and simplified
722 model parameters does not influence the trends in speedup.

723 Computing loads are balanced for all simulations in this study, i.e. the number of river
724 reaches assigned to each processing core is almost identical across cores. Figure 13
725 shows how sub-basins of the Upper Mississippi River Basin are divided among
726 processing cores as well as the longest river path of the basin. The longest path goes
727 through 8 sub-basins on 8 cores, and 14 sub-basins on 16 cores. If one were to apply the
728 traditional Muskingum method on several processing cores with the division in sub-
729 basins shown in Figure 13, computations would have to be made sequentially from
730 upstream to downstream, each core having to wait for its upstream core to be done prior
731 to starting its work. Hence, assuming that the total computing time can be evenly divided
732 by the total number of nodes and neglecting communication overhead, one could only
733 hope to decrease computing time by a factor of $8/8 = 1$ (no gain) for 8 cores and by a
734 factor of $16/14 = 1.14$ for 16 cores. The iterative matrix solver provides much better
735 results (a decrease by a factor of 2.90 for 16 cores).

736 River flow is a causal phenomenon that mainly goes downstream. Therefore, when using
737 an upstream-to-downstream computation scheme and unless dealing with completely
738 separated river basins, one cannot expect to obtain perfect speedup i.e. decreasing of
739 computing time by a factor equal to the number of cores. However, today's
740 supercomputers having tens of thousands of computing cores, one could leverage such
741 power to save human time. Additionally, the matrix method developed here can be
742 directly applied to a combination of independent river basins in which case speedup
743 would be ideally perfect. Furthermore, matrix methods such as the one developed here

744 could be adapted to more complex river flow equations – like variable-parameter
745 Muskingum methods or schemes allowing for backwater effects – in order to save total
746 computing time. Finally, the splitting up into sub-basins used here is very simple and
747 optimizing this partition by limiting connections between sub-basins or taking into
748 account flow wave celerities relatively to basin sizes could respectively help limit the
749 number of communications and the number of iterations in the linear system solver.
750

751 **Conclusions**

752 NHDPlus is a GIS dataset that describes the networks of mapped rivers and water bodies
753 of the United States. One of the main advantages of NHDPlus is that connectivity
754 information for the river networks is available. Therefore, this dataset offers possibilities
755 for the development of river routing models that simultaneously calculate flow and
756 volume of water in all water bodies of the nation. Furthermore, the USGS National
757 Water Information System has thousand of gages located on the NHDPlus network which
758 can be used to assess the quality of such river models across river basins (not only at
759 basin outlets). The research presented in this paper investigates how to develop a river
760 network model using NHDPlus networks and how to assess model computations and
761 optimize model parameters with USGS stream flow measurements. All tools and
762 datasets used herein are available for the contiguous United States, but this research
763 addresses two smaller domains. The combination of the Guadalupe and San Antonio
764 River Basins in Texas is used in a 4-year case study, and the Upper Mississippi River
765 Basin is used in a speedup study with synthetic data. Graph theory is applied to a river
766 network to create a network matrix that is used to develop a vector-matrix version of the
767 Muskingum method and applied in a new river network model called RAPID. It has been
768 shown that a GIS-based hydrographic dataset can be used as the river network for a river
769 model to compute flow in large networks of thousands of reaches, including ungaged
770 locations. A simple flux coupler for connecting a land surface model with an NHDPlus
771 river network is presented. No horizontal routing of flow from the land surface to the
772 river network is used in this study, and such an addition would help improve model
773 calculations. An inverse method is developed to estimate model parameters in RAPID

774 using available gage measurements located across the river basins. Wave celerities are
775 estimated in several locations of the basin studied. RMSE and Nash efficiency of
776 computed flow rates in four RAPID simulations are compared with a basic lumped model
777 where runoff is directly accumulated at the gage, with gage measurements and among
778 themselves. RAPID produces better RMSE and Nash efficiency than the lumped model
779 and the improvements are statistically significant. Although the quality of RAPID
780 calculations is tied to the quantity of runoff generated by the land surface model that
781 provides runoff, mass is conserved within RAPID since the average flow rate is
782 conserved. Spatial variability of parameters enhances the RMSE and Nash efficiency of
783 RAPID calculations. Wave celerities are reproduced within a few percents with the
784 model proposed, although wave celerities closer to those estimated from gage data
785 generally deteriorate the other statistics of calculations. This deterioration might be due
786 to runoff being produced too slowly or too far upstream of each gage. The parameters
787 used in this study are simple, but could be improved based on information available in
788 NHDPlus such as slope, mean flow and velocity of all reaches or by using modified
789 versions of the Muskingum method with time-variable parameters although the latter
790 would necessitate modification of the optimization procedure developed herein. The
791 matrix formulation in RAPID can be transferred in a parallel computing environment. A
792 synthetic study of the Upper Mississippi River Basin shows that although a large initial
793 overhead is added by the matrix method, this overhead decreases with increasing number
794 of processing cores. More importantly, an iterative matrix solver allows de-coupling of
795 sub-basins – even if the main river basin is fully interconnected – hence permitting
796 computation of sub-basins separately if they are distant enough from each other. As

797 consequence, while producing the exact same results as the traditional Muskingum
798 method, the matrix-based Muskingum method decreases the total computing time when
799 run on several processing cores. Such a gain in computing time would be highly
800 beneficial if addressing larger scales, like the entire Contiguous United States which
801 would represent a square matrix of size 3 million.

802

803 **Acknowledgements**

804 This work was partially supported by the U.S. National Aeronautics and Space
805 Administration under the Interdisciplinary Science Project NNX07AL79G, by the U.S.
806 National Science Foundation under project EAR-0413265: CUAHSI Hydrologic
807 Information Systems, by Ecole des Mines de Paris, France, and by the American
808 Geophysical Union under a Horton (Hydrology) Research Grant. The authors wish to
809 thank the PETSc and TAO developers, especially Dr. Barry Smith, Dr. Matthew
810 Knepley, Dr. Satish Balay and Dr. Jason Sarich for their continuous assistance
811 throughout the development of RAPID. Thank you to Dr. Karl Shultz from TACC for
812 his help regarding the handling of inputs and outputs on supercomputers. The computing
813 resources were provided by TACC, which is gratefully acknowledged. Thank you to Dr.
814 Stefano Orlandini for suggestions on an early version of this work. The authors are
815 thankful to the two anonymous reviewers and to the editor for their valuable comments
816 and suggestions that helped improved the original version of this manuscript.

817

818 **Appendix A – Implementation of RAPID**

819 The river network routing model is coded in Fortran 90 using the Portable, Extensible
820 Toolkit for Scientific Computation (PETSc) mathematical library [*Balay, et al., 1997;*
821 *Balay, et al., 2008; Balay, et al., 2009*] and the Toolkit for Advanced Optimization
822 (TAO) optimization library [*McInnes, et al., 2009*]. PETSc can be used to create
823 matrices and vectors and to apply a variety of linear operations such as matrix-vector
824 multiplications or linear system solving. TAO offers multiple methods for unconstrained
825 and constrained optimization. Both PETSc and TAO are built upon the Message Passing
826 Interface [*Dongarra, et al., 1994*] – a standard for communications between processing
827 cores – and can seamlessly be run in a sequential or a parallel computing environment.
828 In this study, sparse matrices are stored using the sequential AIJ format when using one
829 processing core and the MPIAIJ format when using several cores. Linear systems are
830 solved within PETSc either by preconditioning only or with preconditioning associated to
831 a Richardson method. The preconditioning methods used herein are ILU on one
832 processing core, and bloc Jacobi on several cores. The optimization method used in TAO
833 is a line search algorithm called the Nelder-Mead method. The netCDF file format [*Rew*
834 *and Davis, 1990*] is utilized for both inputs and outputs. RAPID is run on single- and
835 multiple-processor workstations as well as on Lonestar
836 (<http://www.tacc.utexas.edu/resources/hpcsystems/#lonestar>), a supercomputer running at
837 the Texas Advanced Computing Center (TACC). This Dell Linux Cluster has 1,460
838 nodes, each node with 8 GB of memory and with two dual-core sockets. Lonestar has a
839 total of 5,840 computing cores.

840

841 **Appendix B – NHDPlus used in RAPID**

842 NHDPlus [USEPA and USGS, 2007] is a geographic information system (GIS) dataset
843 for the hydrography of the United States. This dataset provides the mapped streams and
844 rivers as well as the catchments that surround them. NHDPlus is based on the medium
845 resolution 1:100,000 scale national hydrographic dataset (NHD). One of the main
846 improvements in NHDPlus is the network connectivity available in the value added
847 attributes (VAA) table for the river network. Each NHDPlus reach in the national
848 network is assigned a unique integer identifier called COMID. NHDPlus catchments also
849 have a COMID, the same COMID being used for the reach and its local contributing
850 catchment. Nodes are located at the two ends of each NHDPlus river reach. A unique
851 integer identifier is given to all nodes in the national river reach network. The VAA table
852 includes *FromNode* and *ToNode* fields that give which node is upstream and which is
853 downstream of a given reach. Two reaches that are connected in a river network share a
854 node, and the reach j flows into the reach i if $ToNode(j) = FromNode(i)$. The
855 NHDPlus connectivity between reaches, catchments and nodes is illustrated for three
856 catchments of the Guadalupe and San Antonio basins in Figure 14.
857 In its current formulation, RAPID can handle several upstream reaches but only one
858 unique downstream reach. However, divergences exist in mapped river networks, as they
859 do in NHDPlus. The VAA table offers a *Divergence* field to each of the river reaches
860 (with values of 0 – not part of a divergence, 1 – main path of a divergence, 2 – minor path
861 of a divergence). In the current formulation of RAPID, the main part of a divergence
862 carries all the upstream flow. The *FromNode*, *ToNode* and *Divergence* fields are used to

863 populate the network matrix given in Equation (5), by means of the following logical
864 statement:

865

$$866 \quad \forall (i, j) \in [1, m]^2, \text{ if } [FromNode(i) = ToNode(j)] \text{ and } [Divergence(j) \neq 2] \Rightarrow N_{i,j} = 1 \quad (23)$$

867

868 where $N_{i,j}$ is the element of \mathbf{N} located at row i and column j . Therefore, upstream to
869 downstream connection is conserved if the downstream reach is the major branch of a
870 divergence or if it is not part of a divergence at all, but the connection is not made for a
871 minor branch of a divergence.

872 The VAA table also has information on the relative location – upstream or downstream –
873 of NHDPlus reaches. This information is available in a field called *Hydroseq* consisting
874 of a unique integer attributed to all NHDPlus reaches. Sorting the *Hydroseq* field in
875 decreasing order prior to computations guarantees that all upstream elements are
876 computed prior to solving the flow equations for any given river reach. This organization
877 of computations allows the matrix $\mathbf{I} - \mathbf{C}_1 \cdot \mathbf{N}$ of Equation (1) to be made lower triangular
878 which increases the ease and speed of solving this linear system.

879

880 **References**

- 881 Apostolopoulos, T. K., and K. P. Georgakakos (1997), Parallel computation for
882 streamflow prediction with distributed hydrologic models, *Journal of Hydrology*, 197, 1-
883 24.
- 884 Balay, S., W. D. Gropp, L. C. McInnes, and B. F. Smith (1997), Efficient Management of
885 Parallelism in Object Oriented Numerical Software Libraries, in *Modern Software Tools*
886 *in Scientific Computing*, edited by E. A. a. A. M. B. a. H. P. Langtangen, pp. 163-202.
- 887 Balay, S., K. Buschelman, V. Eijkhout, W. D. Gropp, D. Kaushik, M. G. Knepley, L. C.
888 McInnes, B. F. Smith, and H. Zhang (2008), PETSc Users Manual (Revision 3.0.0), 1-
889 191 pp, Argonne National Laboratory.
- 890 Balay, S., K. Buschelman, W. D. Gropp, D. Kaushik, M. G. Knepley, L. C. McInnes, B.
891 F. Smith, and H. Zhang (2009), PETSc Web page, Available online at
892 <http://www.mcs.anl.gov/petsc>.
- 893 Berge, C. (1958), Matrice Associée d'un graphe, in *Théorie des Graphes et ses*
894 *Applications*, edited, pp. 126-128, Dunod, Paris.
- 895 Cunge, J. A. (1969), On the subject of a flood propagation computation method
896 (Muskingum method), *Journal of Hydraulic Research*, 7, 205-230.
- 897 David, C. H., D. J. Gochis, D. R. Maidment, W. Yu, D. N. Yates, and Z.-L. Yang (2009),
898 Using NHDPlus as the Land Base for the Noah-distributed Model, *Transactions in GIS*,
899 13, 363-377.
- 900 De Roo, A., B. Gouweleeuw, and J. Thielen (2003), Development of a European flood
901 forecasting system, *International Journal of River Basin Management*, 1, 49-59.
- 902 Dongarra, J., D. Walker, E. Lusk, B. Knighten, M. Snir, A. Geist, S. Otto, R. Hempel, E.
903 Lusk, W. Gropp, J. Cownie, T. Skjellum, L. Clarke, R. Littlefield, M. Sears, S.
904 Husslederman, E. Anderson, S. Berryman, J. Feeney, D. Frye, L. Hart, A. Ho, J. Kohl, P.
905 Madams, C. Mosher, P. Pierce, E. Schikuta, R. G. Voigt, R. Babb, R. Bjornson, V.
906 Fernando, I. Glendinning, T. Haupt, C. T. H. Ho, S. Krauss, A. Mainwaring, D. Nessel, S.
907 Ranka, A. Singh, D. Weeks, J. Baron, N. Doss, S. Fineberg, A. Greenberg, D. Heller,
908 G. Howell, B. Leary, O. McBryan, P. Pacheco, P. Rigsbee, A. Sussman, S. Wheat, E.
909 Barszcz, A. Elster, J. Flower, R. Harrison, T. Henderson, J. Kapenga, A. Maccabe, P.
910 McKinley, H. Palmer, A. Robison, R. Tomlinson, and S. Zenith (1994), Special Issue -
911 MPI - a Message-Passing Interface Standard, *International Journal of Supercomputer*
912 *Applications and High Performance Computing*, 8, 159-416.
- 913 Fread, D. L. (1993), Flow Routing, in *Handbook of Hydrology*, edited by D. R.
914 Maidment, pp. 10.17-10.18, McGraw-Hill, New York.
- 915 Gochis, D. J., and F. Chen (2003), Hydrological Enhancements to the Community Noah
916 Land Surface Model, available online at
917 <http://www.ucar.edu/library/collections/technotes/technotes.jsp>.
- 918 Guan, H., J. L. Wilson, and H. Xie (2009), A cluster-optimizing regression-based
919 approach for precipitation spatial downscaling in mountainous terrain, *Journal of*
920 *Hydrology*, 375, 578-588.
- 921 Habets, F., J. Noilhan, C. Golaz, J. P. Goutorbe, P. Lacarrere, E. Martin, C. Oettle, and D.
922 Vidal-Madjar (1999a), The ISBA surface scheme in a macroscale hydrological model

923 applied to the Hapex-Mobilhy area - Part I: Model and database, *Journal of Hydrology*,
924 217, 75-96.

925 Habets, F., J. Noilhan, C. Golaz, J. P. Goutorbe, P. Lacarrere, E. Leblois, E. Ledoux, E.
926 Martin, C. Otle, and D. Vidal-Madjar (1999b), The ISBA surface scheme in a
927 macroscale hydrological model applied to the Hapex-Mobilhy area - Part II: Simulation
928 of streamflows and annual water budget, *Journal of Hydrology*, 217, 97-118.

929 Habets, F., P. Etchevers, C. Golaz, E. Leblois, E. Ledoux, E. Martin, J. Noilhan, and C.
930 Otle (1999c), Simulation of the water budget and the river flows of the Rhone basin,
931 *Journal of Geophysical Research-Atmospheres*, 104, 31145-31172.

932 Habets, F., A. Boone, J. L. Champeaux, P. Etchevers, L. Franchisteguy, E. Leblois, E.
933 Ledoux, P. Le Moigne, E. Martin, S. Morel, J. Noilhan, P. Q. Segui, F. Rousset-
934 Regimbeau, and P. Vienne (2008), The SAFRAN-ISBA-MODCOU
935 hydrometeorological model applied over France, *Journal of Geophysical Research-
936 Atmospheres*, 113.

937 Helsel, D. R., and R. M. Hirsch (2002), Chapter A3. Statistical Methods in Water
938 Resources, in *Techniques of Water-Resources Investigations of the United States
939 Geological Survey. Book 4, Hydrologic Analysis and Interpretation*, edited, pp. 137-156,
940 United States Geological Survey.

941 Jones, J. E., and C. S. Woodward (2001), Newton-Krylov-multigrid solvers for large-
942 scale, highly heterogeneous, variably saturated flow problems, *Advances in Water
943 Resources*, 24, 763-774.

944 Kollet, S. J., and R. M. Maxwell (2006), Integrated surface-groundwater flow modeling:
945 A free-surface overland flow boundary condition in a parallel groundwater flow model,
946 *Advances in Water Resources*, 29, 945-958.

947 Kollet, S. J., R. M. Maxwell, C. S. Woodward, S. Smith, J. Vanderborcht, H. Vereecken,
948 and C. Simmer (2010), Proof of concept of regional scale hydrologic simulations at
949 hydrologic resolution utilizing massively parallel computer resources, *Water Resour.
950 Res.*, 46, W04201.

951 Koussis, A. D. (1978), Theoretical Estimations of Flood Routing Parameters, *J. Hydraul.
952 Div. Am. Soc. Civ. Eng.*, 104, 109-115.

953 Larson, J. W., A. P. Craig, J. B. Drake, D. J. I. Erickson, M. Branstetter, and M. W. Ham
954 (2007), A Massively Parallel Dynamical Core for Continental- to Global-Scale River
955 Transport, paper presented at Proceedings of the International Congress and Modelling
956 and Simulation (ModSim 2007).

957 Ledoux, E., G. Girard, G. de Marsily, J. P. Villeneuve, and J. Deschenes (1989), Spatially
958 Distributed Modeling: Conceptual Approach, Coupling Surface Water and Groundwater,
959 in *Unsaturated Flow in Hydrologic Modeling Theory and Practice*, edited by H. J.
960 Morel-Seytoux, pp. 435-454, Kluwer Academic Publishers.

961 Lehner, B., K. Verdin, and A. Jarvis (2006), HydroSHEDS Technical Documentation,
962 available online at <http://hydrosheds.cr.usgs.gov>.

963 Leopold, C., M. Süß, and J. Breitbart (2006), Programming for Malleability with Hybrid
964 MPI-2 and OpenMP: Experiences with a Simulation Program for Global Water
965 Prognosis, paper presented at European Conference on Modelling and Simulation.

966 Lohmann, D., E. Raschke, B. Nijssen, and D. P. Lettenmaier (1998a), Regional scale
967 hydrology: I. Formulation of the VIC-2L model coupled to a routing model, *Hydrological*
968 *Sciences Journal-Journal Des Sciences Hydrologiques*, 43, 131-141.

969 Lohmann, D., E. Raschke, B. Nijssen, and D. P. Lettenmaier (1998b), Regional scale
970 hydrology: II. Application of the VIC-2L model to the Weser River, Germany,
971 *Hydrological Sciences Journal-Journal Des Sciences Hydrologiques*, 43, 143-158.

972 Lohmann, D., K. E. Mitchell, P. R. Houser, E. F. Wood, J. C. Schaake, A. Robock, B. A.
973 Cosgrove, J. Sheffield, Q. Y. Duan, L. F. Luo, R. W. Higgins, R. T. Pinker, and J. D.
974 Tarpley (2004), Streamflow and water balance intercomparisons of four land surface
975 models in the North American Land Data Assimilation System project, *Journal of*
976 *Geophysical Research-Atmospheres*, 109, 1-22.

977 Maurer, E. P., G. M. O'Donnell, D. P. Lettenmaier, and J. O. Roads (2001), Evaluation of
978 the land surface water budget in NCEP/NCAR and NCEP/DOE reanalyses using an off-
979 line hydrologic model, *Journal of Geophysical Research-Atmospheres*, 106, 17841-
980 17862.

981 McCarthy, G. T. (1938), The Unit Hydrograph and Flood Routing, paper presented at
982 Conference of the North Atlantic Division, U.S. Engineer Department, New London,
983 Connecticut, on June 24, 1938.

984 McInnes, L. C., J. Moré, T. Munson, and J. Sarich (2009), TAO User Manual (Revision
985 1.10), 1-64 pp, Mathematics and Computer Science Division, Argonne National
986 Laboratory, Available online at <http://www.mcs.anl.gov/tao>.

987 Miller, W. A., and J. A. Cunge (1975), Simplified Equations of Unsteady Flow, in
988 *Unsteady Flow in Open Channels*, edited by K. Mahmood and V. Yevjevich, pp. 216-
989 232, Water Resources Publications, Fort Collins, CO.

990 Nash, J. E., and J. V. Sutcliffe (1970), River flow forecasting through conceptual models
991 part I -- A discussion of principles, *Journal of Hydrology*, 10, 282-290.

992 NERC (1975), Flood Routing Studies, in *Flood Studies Report*, edited, National
993 Environment Research Council, London.

994 Niu, G. Y., Z. L. Yang, R. E. Dickinson, L. E. Gulden, and H. Su (2007), Development of
995 a simple groundwater model for use in climate models and evaluation with Gravity
996 Recovery and Climate Experiment data, *Journal of Geophysical Research-Atmospheres*,
997 112, 1-14.

998 Niu, G. Y., Z. L. Yang, K. E. Mitchell, F. Chen, M. Ek, M. Barlage, L. Longuevergne, A.
999 Kumar, K. Manning, D. Niyogi, E. Rosero, M. Tewari, and Y.-L. Xia (2010), The
1000 Community Noah Land Surface Model with Multi-Physics Options, *Journal of*
1001 *Geophysical Research-Atmospheres*, (submitted).

1002 Oki, T., Y. Agata, S. Kanae, T. Saruhashi, D. W. Yang, and K. Musiake (2001), Global
1003 assessment of current water resources using total runoff integrating pathways,
1004 *Hydrological Sciences Journal-Journal Des Sciences Hydrologiques*, 46, 983-995.

1005 Olivera, F., J. Famiglietti, and K. Asante (2000), Global-scale flow routing using a
1006 source-to-sink algorithm, *Water Resources Research*, 36, 2197-2207.

1007 Orlandini, S., and R. Rosso (1998), Parameterization of stream channel geometry in the
1008 distributed modeling of catchment dynamics, *Water Resources Research*, 34, 1971-1985.

1009 Orlandini, S., G. Moretti, M. Franchini, B. Aldighieri, and B. Testa (2003), Path-based
1010 methods for the determination of nondispersive drainage directions in grid-based digital
1011 elevation models, *Water Resources Research*, 39.
1012 Ponce, V. M., and V. Yevjevich (1978), Muskingum-Cunge Method with Variable
1013 Parameters, *J. Hydraul. Div. Am. Soc. Civ. Eng.*, 104, 1663-1667.
1014 Ponce, V. M. (1986), Diffusion Wave Modeling of Catchment Dynamics, *J. Hydraul.*
1015 *Eng.-ASCE*, 112, 716-727.
1016 Rew, R., and G. Davis (1990), Netcdf - an Interface for Scientific-Data Access, *Ieee*
1017 *Computer Graphics and Applications*, 10, 76-82.
1018 Solomon, S., D. Qin, M. Manning, Z. Chen, M. Marquis, K.B. Averyt, M. Tignor, and H.
1019 L. Miller (2007), *Climate Change 2007: The Physical Science Basis. Contribution of*
1020 *Working Group I to the Fourth Assessment Report of the Intergovernmental Panel on*
1021 *Climate Change (IPCC)*, 996 pp., Cambridge University Press, Cambridge.
1022 Todini, E. (2007), A mass conservative and water storage consistent variable parameter
1023 Muskingum-Cunge approach (vol 11, pg 1645, 2007), *Hydrology and Earth System*
1024 *Sciences*, 11, 1783-1783.
1025 USEPA, and USGS (2007), NHDPlus User Guide, available online at
1026 <http://www.horizon-systems.com/nhdplus/documentation.php>.
1027 von Bloh, W., S. Rost, D. Gerten, and W. Lucht (2010), Efficient parallelization of a
1028 dynamic global vegetation model with river routing, *Environmental Modelling &*
1029 *Software*, 25, 685-690.
1030 Wilcoxon, F. (1945), Individual Comparisons by Ranking Methods, *Biometrics Bulletin*,
1031 1, 80-83.
1032
1033

Table 1 Travel time (s) for the flow waves estimated using the lagged cross-correlation in the Guadalupe and San Antonio River Basins, both from IDA measurements and from RAPID model runs; and distance (km) between gaging stations

		Location of the two consecutive streamflow gages										
		Ingram - Kerrville	Kerrville - Comfort	Comfort - Spring Branch	Sattler - Gonzales	Gonzales - Cuero	Cuero - Victoria	Schroeder - Victoria	Bandera - Macdona	Macdona - Elmendorf	Elmendorf - Falls City	Falls City - Goliad
Travel time (s) from IDA	2004	7200	18900	60300	162900	132300	70200	0	20700	0	126000	162000
	2007	6300	18900	59400	131400	108900	70200	8100	37800	15300	91800	126000
	average	6750	18900	59850	147150	120600	70200	4050	29250	7650	108900	144000
Travel time (s) from RAPID outputs	RAPID (k^α, x^α)	6300	8100	35100	90000	29700	38700	5400	50400	29700	22500	52200
	RAPID (k^β, x^β)	6300	8100	46800	128700	84600	36000	4500	24300	8100	91800	124200
	RAPID (k^γ, x^γ)	4500	6300	27900	88200	60300	31500	2700	15300	6300	58500	80100
	RAPID (k^δ, x^δ)	9000	9000	72900	174600	117900	75600	5400	37800	16200	140400	193500
Distance (km)		13.77	40.40	100.85	203.50	110.72	100.71	24.44	116.36	71.73	79.16	137.16

Table 2 Wave celerities (m/s) estimated using the lagged cross-correlation in the Guadalupe and San Antonio River Basins, both from IDA measurements and from RAPID model runs

Wave celerity (m/s)		Location of the two consecutive streamflow gages										
		Ingram - Kerrville	Kerrville - Comfort	Comfort - Spring Branch	Sattler - Gonzales	Gonzales - Cuero	Cuero - Victoria	Schroeder - Victoria	Bandera - Macdona	Macdona - Elmendorf	Elmendorf - Falls City	Falls City - Goliad
from IDA	2004	1.91	2.14	1.67	1.25	0.84	1.43	∞	5.62	∞	0.63	0.85
	2007	2.19	2.14	1.70	1.55	1.02	1.43	3.02	3.08	4.69	0.86	1.09
	average	2.05	2.14	1.69	1.40	0.93	1.43	3.02	4.35	4.69	0.75	0.97
from RAPID outputs	RAPID (k^α, x^α)	2.19	4.99	2.87	2.26	3.73	2.60	4.53	2.31	2.41	3.52	2.63
	RAPID (k^β, x^β)	2.19	4.99	2.16	1.58	1.31	2.80	5.43	4.79	8.85	0.86	1.10
	RAPID (k^γ, x^γ)	3.06	6.41	3.61	2.31	1.84	3.20	9.05	7.61	11.38	1.35	1.71
	RAPID (k^δ, x^δ)	1.53	4.49	1.38	1.17	0.94	1.33	4.53	3.08	4.43	0.56	0.71

Table 3 Comparison of observed and simulated flows at fifteen locations within the Guadalupe and San Antonio River

Basins

Gaging station	Average daily stream flow (m3/s)						Flow ratio	RMS error (m3/s) using daily averages					Nas
	Observed	Lumped	RAPID (k^α, x^α)	RAPID (k^β, x^β)	RAPID (k^γ, x^γ)	RAPID (k^δ, x^δ)	Observed/Lumped	Lumped	RAPID (k^α, x^α)	RAPID (k^β, x^β)	RAPID (k^γ, x^γ)	RAPID (k^δ, x^δ)	
Johnson Ck nr Ingram, TX	1.16	0.06	0.06	0.06	0.06	0.06	19.33	4.41	4.41	4.41	4.41	4.41	-0
Guadalupe Rv at Kerrville, TX	4.15	0.14	0.14	0.14	0.14	0.14	29.64	15.04	15.04	15.04	15.04	15.04	-0
Guadalupe Rv at Comfort, TX	9.97	0.81	0.81	0.81	0.81	0.81	12.31	26.57	26.51	26.51	26.52	26.53	-0
Guadalupe Rv nr Spring Branch, TX	19.74	5.91	5.91	5.91	5.91	5.91	3.34	42.09	43.06	43.48	42.72	44.80	0
Guadalupe Rv at Sattler, TX	22.04	6.62	6.62	6.62	6.62	6.62	3.33	40.08	39.85	39.77	39.94	39.57	-0
Guadalupe Rv at Gonzales, TX	64.28	23.27	23.27	23.27	23.27	23.27	2.76	79.83	80.93	86.44	80.40	93.78	0
Guadalupe Rv at Cuero, TX	73.23	52.63	52.62	52.61	52.62	52.60	1.39	76.86	56.41	64.91	55.52	82.74	0
Guadalupe Rv nr Victoria	80.96	61.95	61.93	61.92	61.93	61.91	1.31	93.97	70.11	65.07	68.05	89.06	0
Coleto Ck at Arnold Rd nr Schroeder, TX	3.45	8.78	8.78	8.78	8.78	8.78	0.39	15.43	15.44	15.45	15.46	15.44	0
Coleto Ck nr Victoria, TX	3.99	13.72	13.72	13.72	13.72	13.72	0.29	21.82	22.61	22.46	22.26	22.65	0
Medina Rv at Banderas, TX	5.30	0.75	0.75	0.75	0.75	0.75	7.07	10.78	10.77	10.77	10.77	10.77	0
Medina Rv nr Macdona, TX	8.73	2.09	2.09	2.09	2.09	2.09	4.18	12.89	12.74	12.72	12.74	12.72	0
San Antonio Rv nr Elmendorf, TX	25.05	7.95	7.95	7.95	7.95	7.95	3.15	39.91	39.27	39.23	39.41	39.16	0
San Antonio Rv nr Falls City, TX	25.01	12.36	12.36	12.36	12.36	12.36	2.02	33.23	31.13	30.63	31.26	32.00	0
San Antonio Rv at Goliad, TX	37.54	34.96	34.95	34.95	34.95	34.94	1.07	42.34	37.73	34.58	36.92	39.10	0
Mean	25.64	15.47	15.46	15.46	15.46	15.46		37.02	33.73	34.10	33.43	37.85	0

Table 4 Results of the Wilcoxon signed-ranks test applied to fifteen stations for efficiency and RMSE and to various routing procedures

Efficiency							
x	y	Number of non-zero differences	Total rank	W ⁺ (computed for y-x)	p-value corresponding to W ⁺	W ⁻ (computed for y-x)	p-value corresponding to W ⁻
Lumped runoff	RAPID (k ^α ,x ^α)	11	66	51.0	0.06152	15.0	0.94922
Lumped runoff	RAPID (k ^β ,x ^β)	11	66	47.0	0.12012	19.0	0.89697
Lumped runoff	RAPID (k ^γ ,x ^γ)	11	66	51.0	0.06152	15.0	0.94922
Lumped runoff	RAPID (k ^δ ,x ^δ)	10	55	22.5	0.70459	32.5	0.33008
RAPID (k ^α ,x ^α)	RAPID (k ^γ ,x ^γ)	10	55	37.0	0.18750	18.0	0.83887
RAPID (k ^β ,x ^β)	RAPID (k ^γ ,x ^γ)	10	55	28.5	0.48047	26.5	0.55811
RAPID (k ^γ ,x ^γ)	RAPID (k ^δ ,x ^δ)	12	78	13.0	0.98291	65.0	0.02124

RMSE							
x	y	Number of non-zero differences	Total rank	W ⁺ (computed for y-x)	p-value corresponding to W ⁺	W ⁻ (computed for y-x)	p-value corresponding to W ⁻
Lumped runoff	RAPID (k ^α ,x ^α)	13	91	25.5	0.92145	65.5	0.08966
Lumped runoff	RAPID (k ^β ,x ^β)	13	91	26.0	0.91614	65.0	0.09546
Lumped runoff	RAPID (k ^γ ,x ^γ)	13	91	25.0	0.92676	66.0	0.08386
Lumped runoff	RAPID (k ^δ ,x ^δ)	13	91	42.5	0.59345	48.5	0.43299
RAPID (k ^α ,x ^α)	RAPID (k ^γ ,x ^γ)	11	66	15.0	0.94922	51.0	0.06152
RAPID (k ^β ,x ^β)	RAPID (k ^γ ,x ^γ)	12	78	41.0	0.45483	37.0	0.57495

RAPID (k^{γ}, x^{γ})	RAPID (k^{δ}, x^{δ})	12	78	64.0	0.02612	14.0	0.97876
------------------------------------	------------------------------------	----	----	------	---------	------	---------

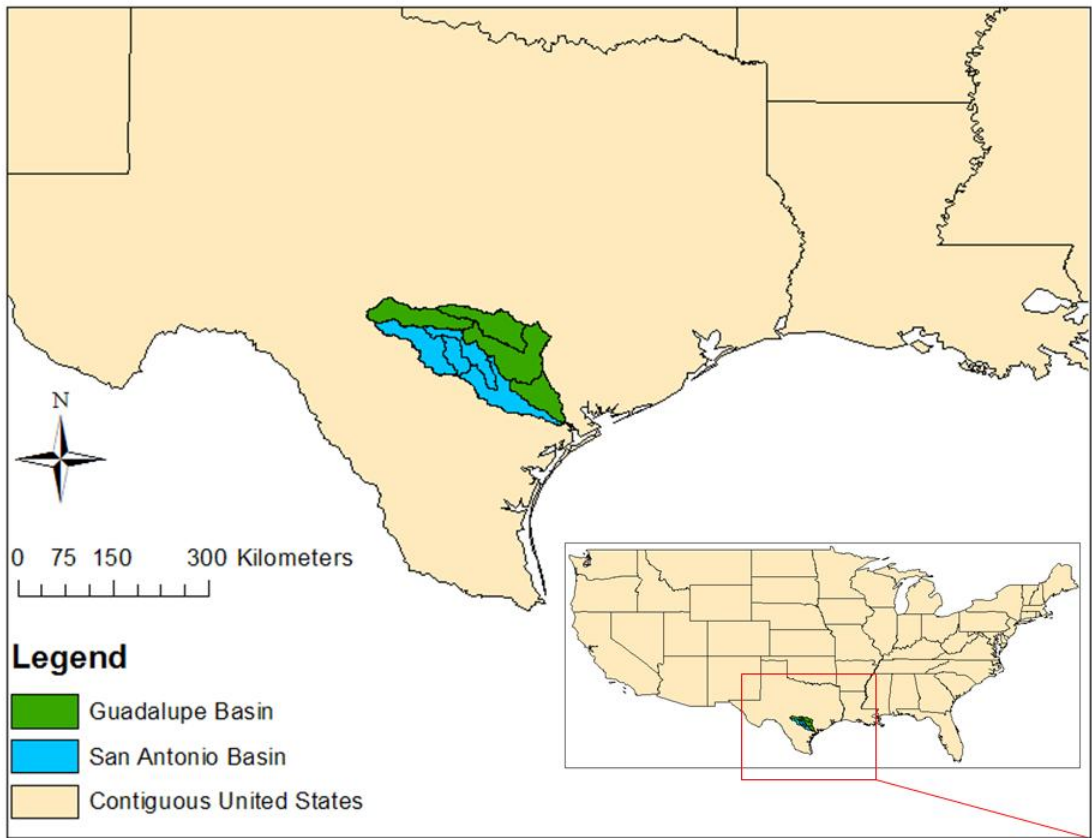


Figure 1 Guadalupe and San Antonio Basins

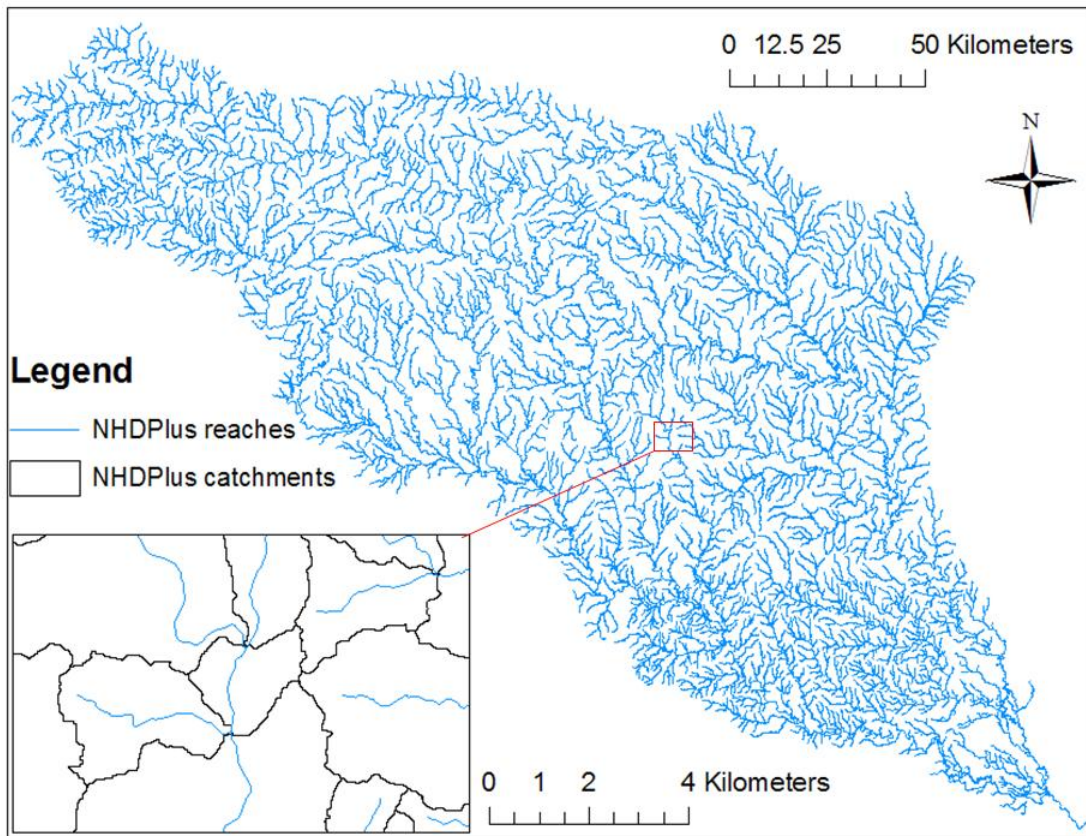


Figure 2 NHDPlus river network and catchments for the Guadalupe and San Antonio Basins

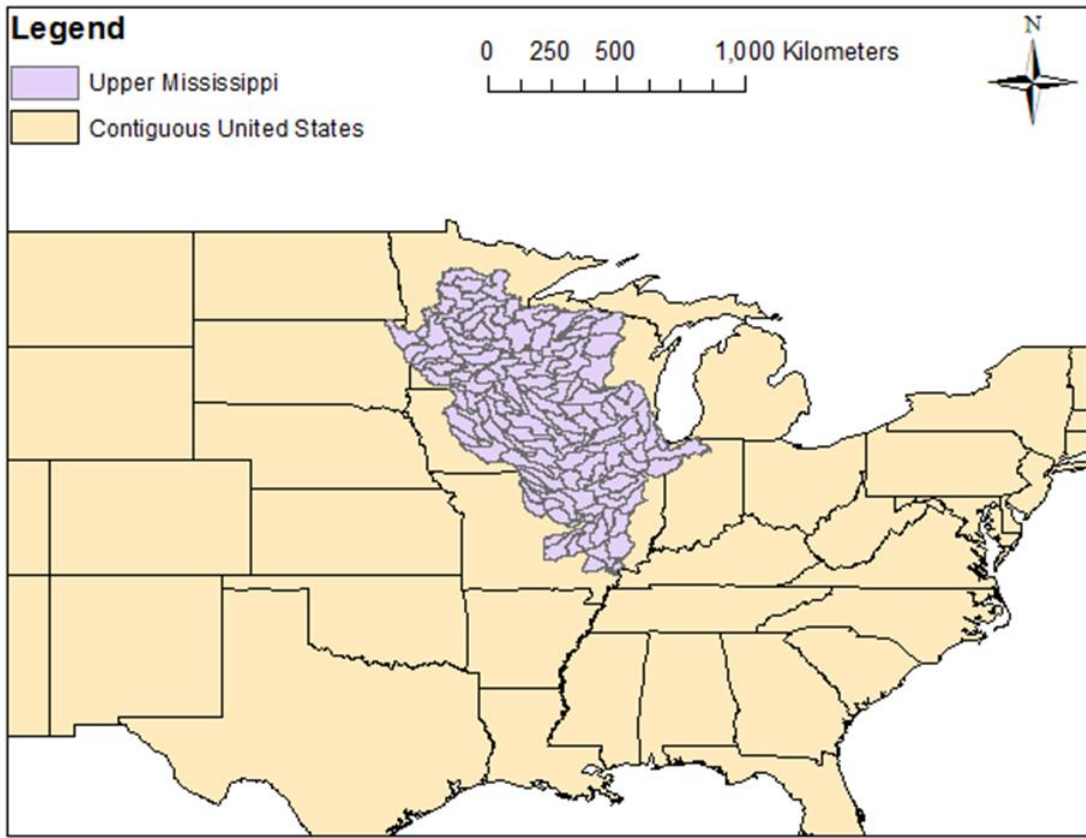


Figure 3 Upper Mississippi River Basin

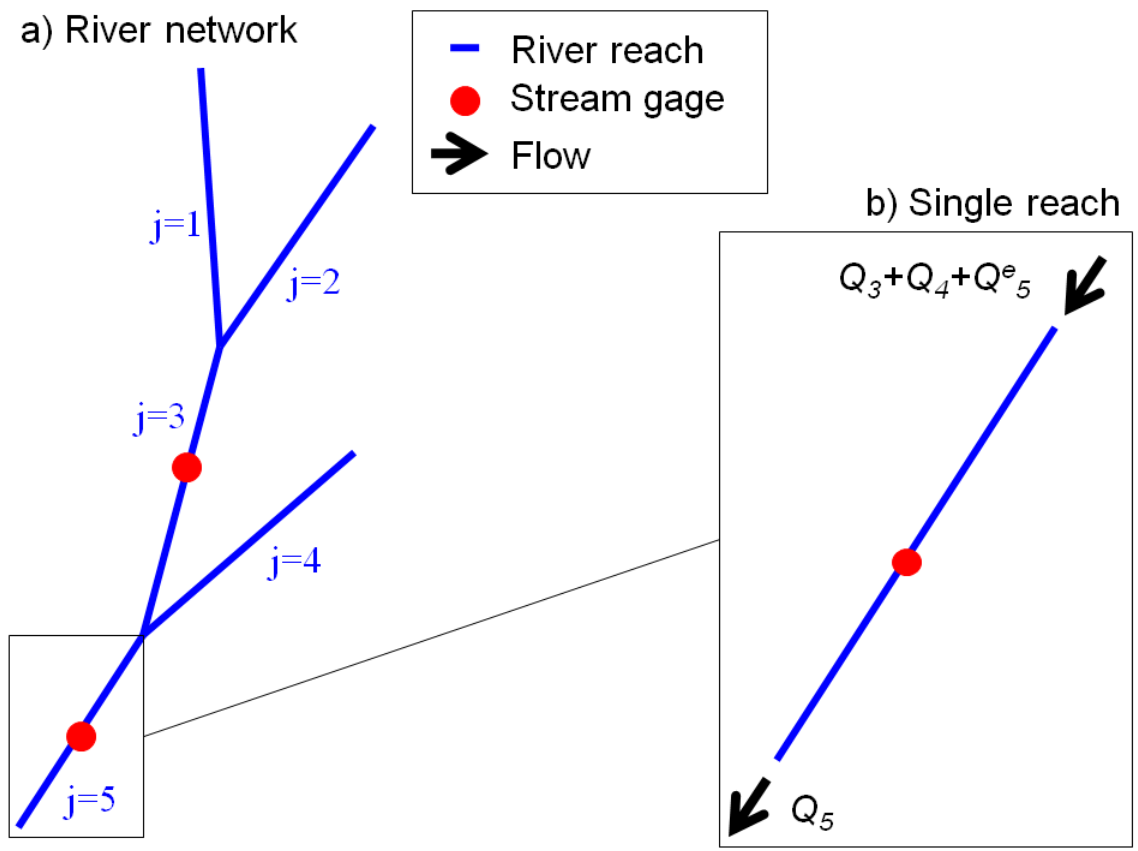


Figure 4 River network

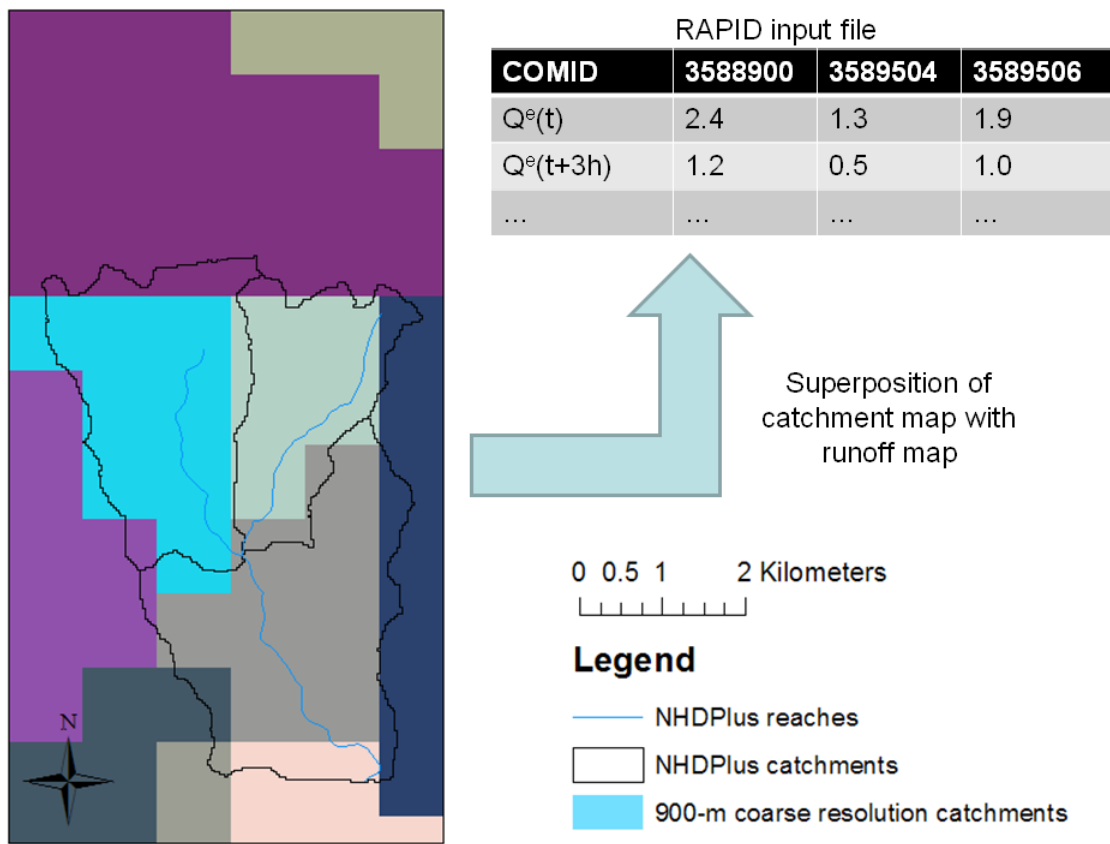


Figure 5 Principle of flux coupler between Noah and RAPID

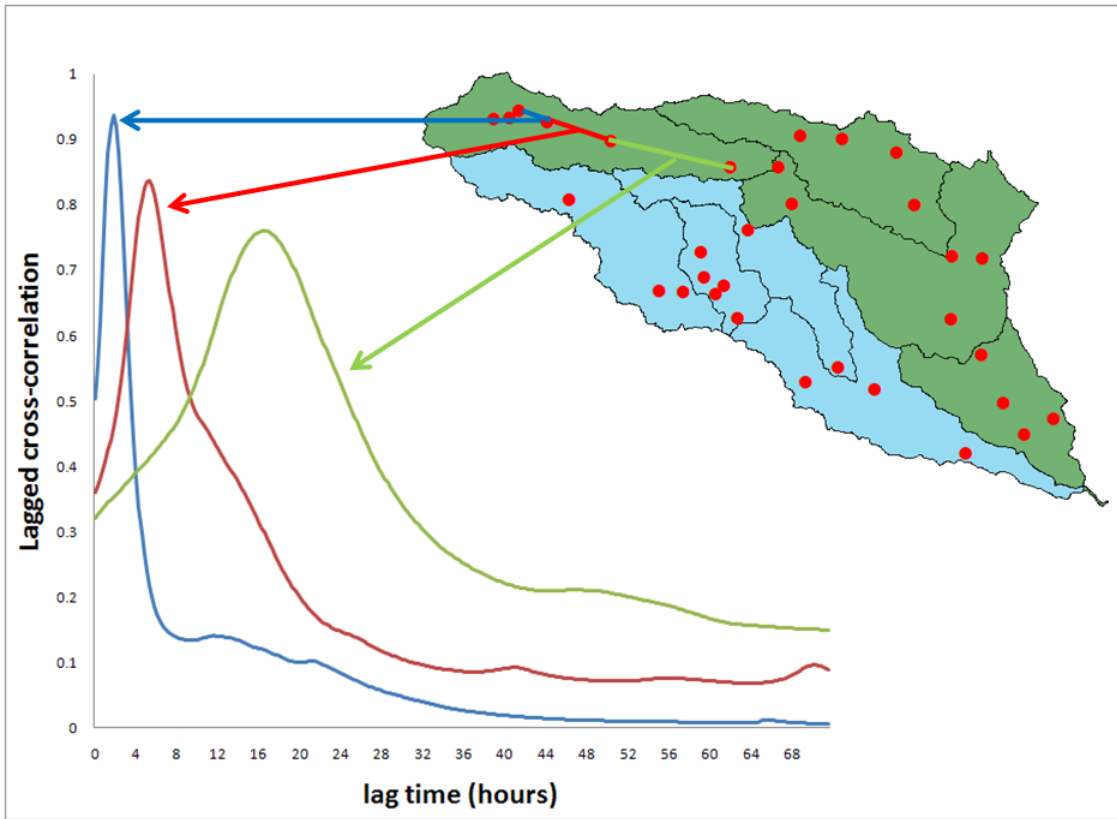


Figure 6 Lagged cross-correlation as a function of lag time

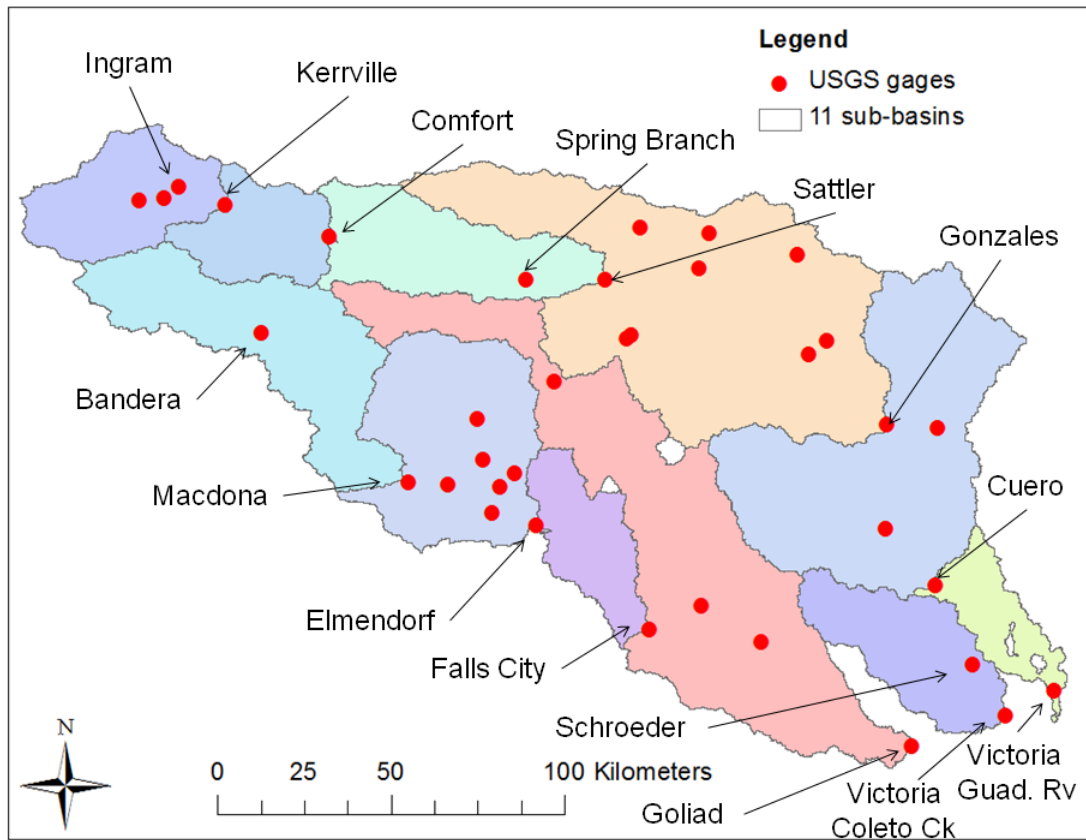


Figure 7 Wave celerities are estimated for eleven different sub-basins within the Guadalupe and San Antonio river basins. Location of 36 gaging stations used for optimization and names of the 15 gaging stations used for estimation of wave celerities. The same sub-basins are used for distributed parameters in RAPID

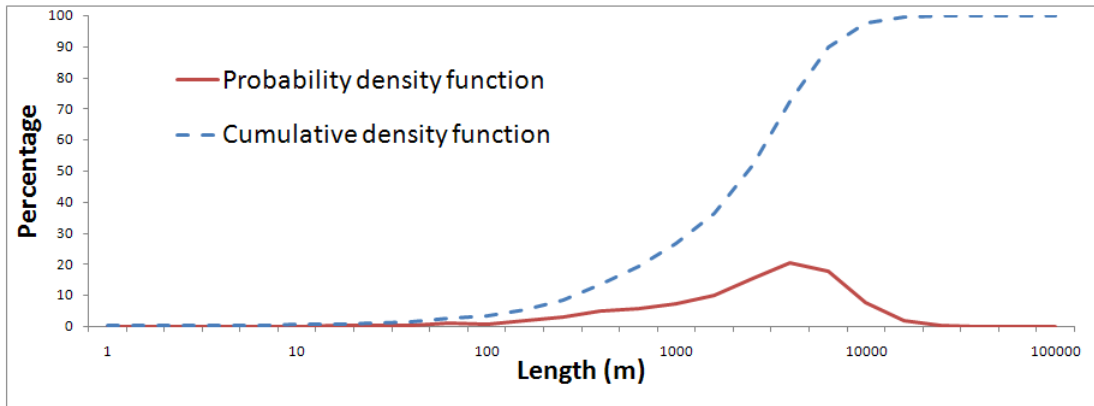


Figure 8 Statistics of river reach lengths in Guadalupe and San Antonio River Basins

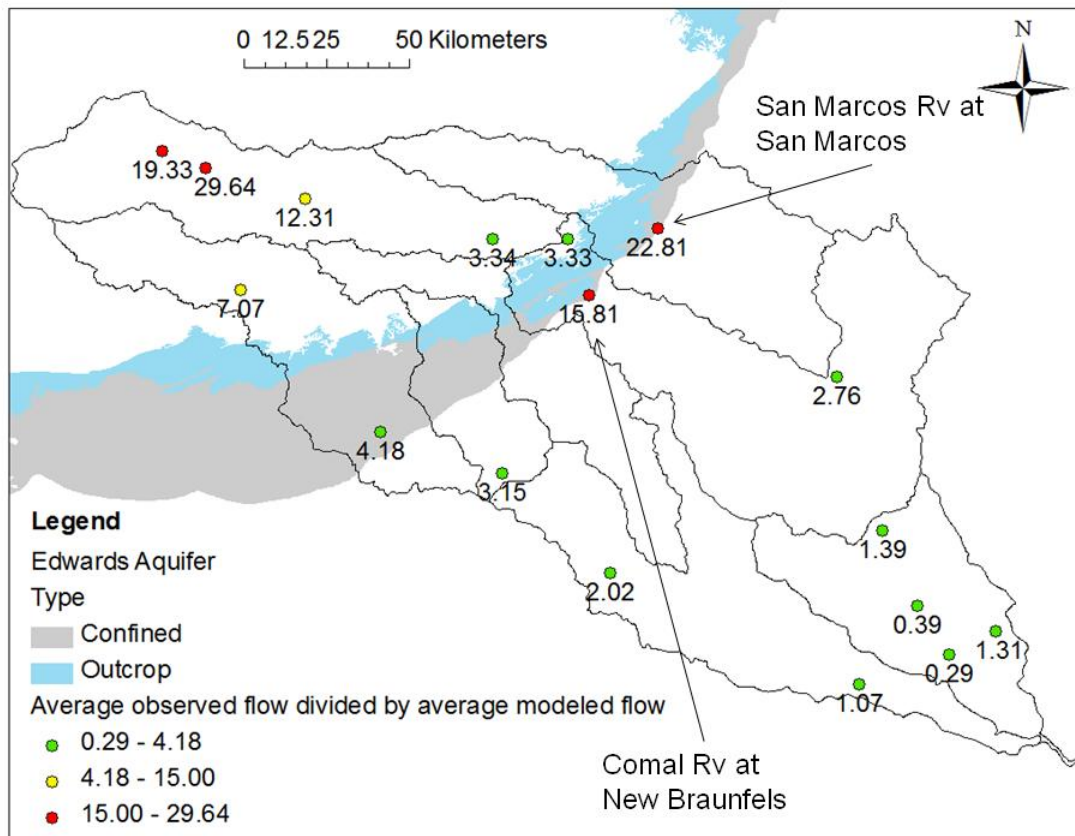


Figure 9 Ratio between observed and modeled stream flow at 16 gages, location of the Edwards Aquifer. Location of the two largest springs in Texas.

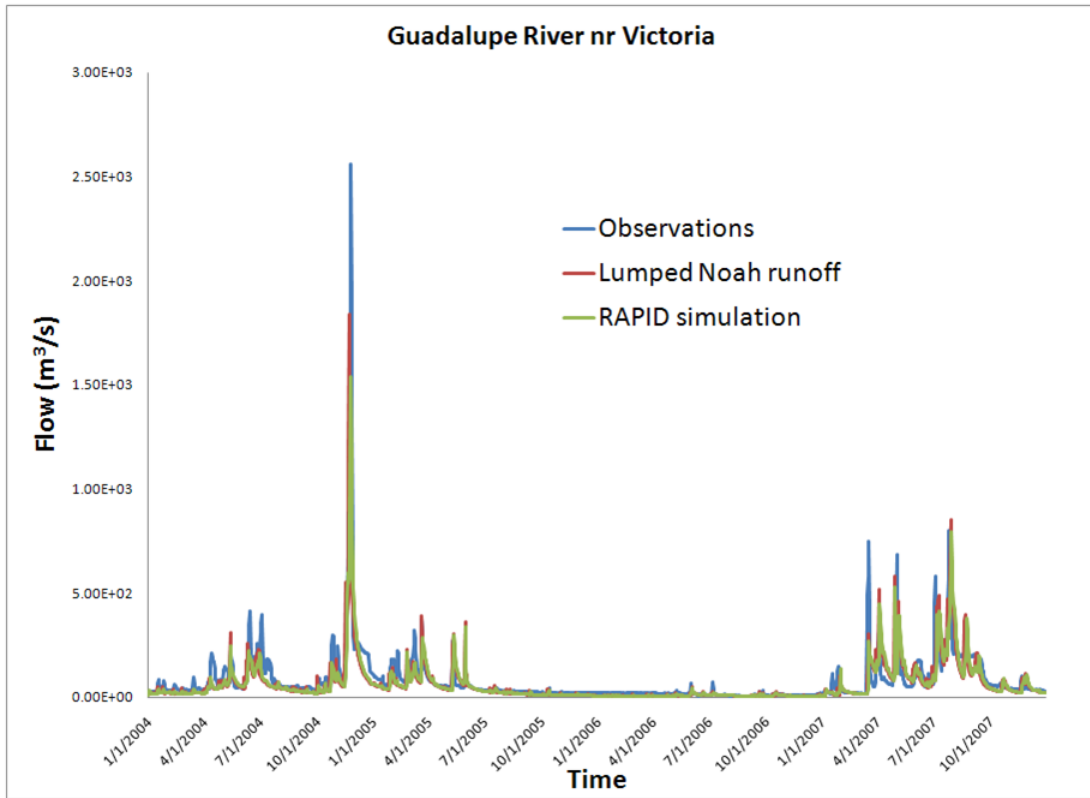


Figure 10 Hydrograph of observed, lumped and routed flows for the Guadalupe River near Victoria, using (k^y, x^y)

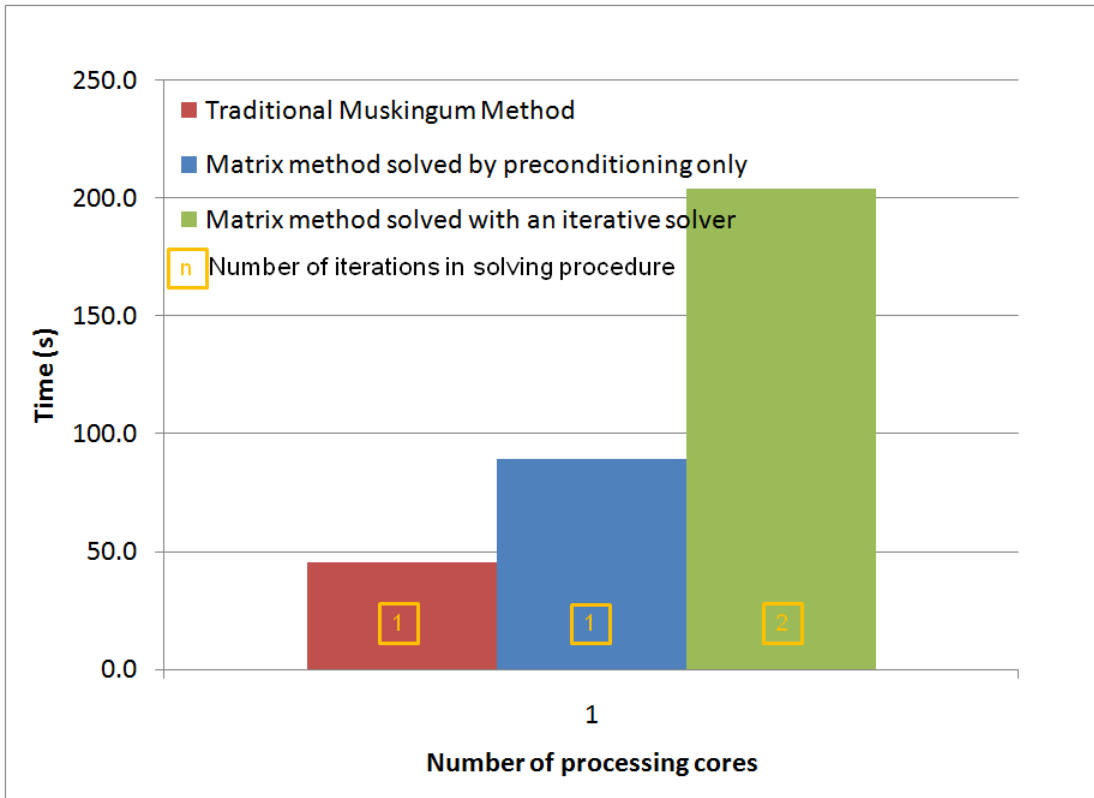


Figure 11 Comparison of computing time between the traditional Muskingum method and matrix methods

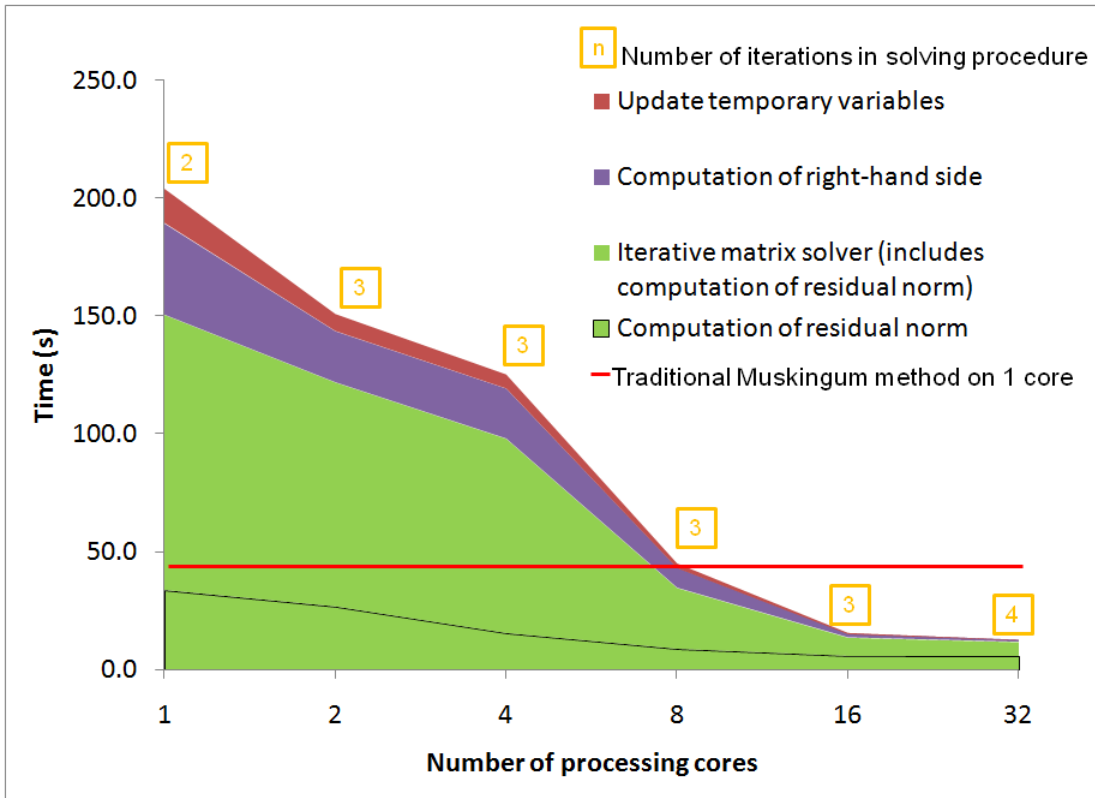


Figure 12 Total computing time for matrix method with an iterative solver as a function of the number of processing cores, number of iterations needed, total computing time for the traditional Muskingum method.

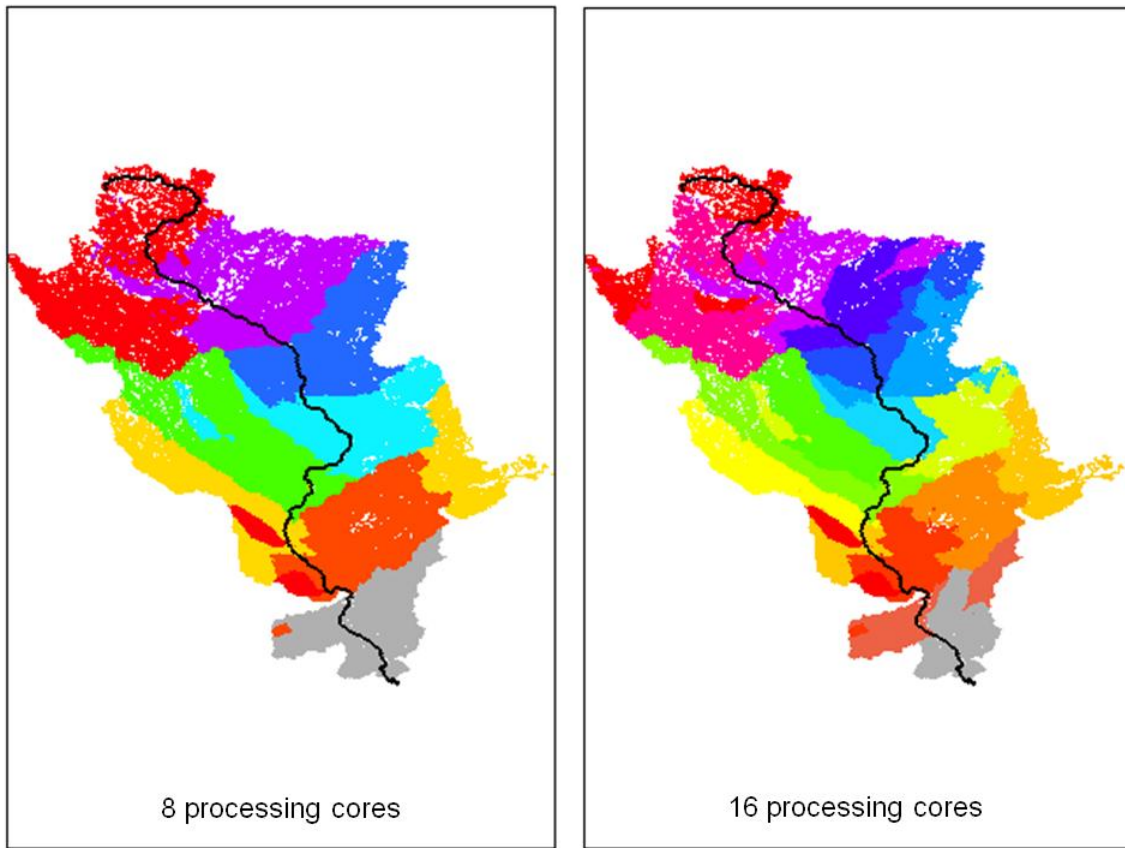


Figure 13 Longest path in the Upper Mississippi River Basin and location of sub-basins when RAPID is used in a parallel computing environment with 8 and 16 processing cores, different colors correspond to different cores.

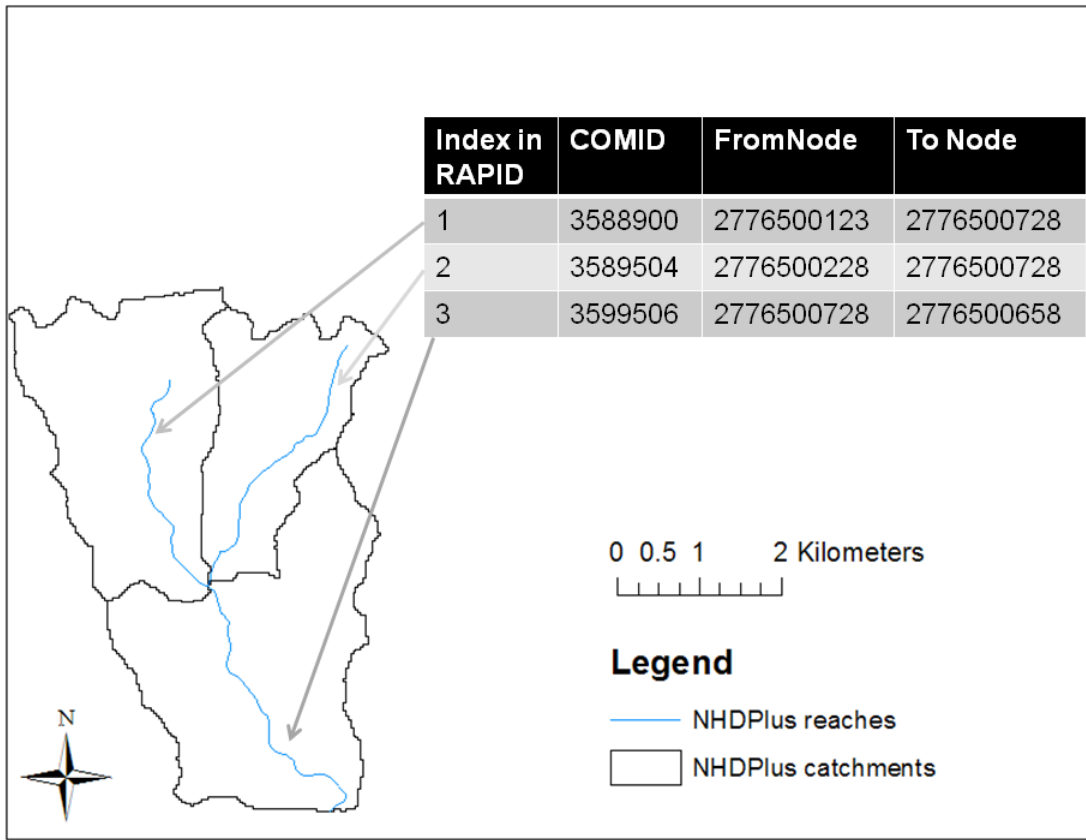


Figure 14 NHDPlus connectivity between reaches, nodes and catchments

Figure captions

Figure 1 Guadalupe and San Antonio Basins

Figure 2 NHDPlus river network and catchments for the Guadalupe and San Antonio Basins

Figure 3 Upper Mississippi River Basin

Figure 4 River network

Figure 5 Principle of flux coupler between Noah and RAPID

Figure 6 Lagged cross-correlation as a function of lag time

Figure 7 Wave celerities are estimated for eleven different sub-basins within the Guadalupe and San Antonio river basins. Location of 36 gaging stations used for optimization and names of the 15 gaging stations used for estimation of wave celerities.

The same sub-basins are used for distributed parameters in RAPID

Figure 8 Statistics of river reach lengths in Guadalupe and San Antonio River Basins

Figure 9 Ratio between observed and modeled stream flow at 16 gages, location of the Edwards Aquifer. Location of the two largest springs in Texas.

Figure 10 Hydrograph of observed, lumped and routed flows for the Guadalupe River near Victoria, using (k^y, x^y)

Figure 11 Comparison of computing time between the traditional Muskingum method and matrix methods

Figure 12 Total computing time for matrix method with an iterative solver as a function of the number of processing cores, number of iterations needed, total computing time for the traditional Muskingum method.

Figure 13 Longest path in the Upper Mississippi River Basin and location of sub-basins when RAPID is used in a parallel computing environment with 8 and 16 processing cores, different colors correspond to different cores.

Figure 14 NHDPlus connectivity between reaches, nodes and catchments